



RESEARCH ARTICLE

Experimental study of induction generator as a repowering solution

Alana S. Magalhaes^{1,2,3}  | Junio S. Bulhoes^{1,2} | Marcio R. C. Reis^{1,2,3} |
Viviane M. Gomes^{1,2,3} | Alan H. F. Silva^{1,2,3} | Aylton J. Alves¹ |
Gabriel A. Wainer³ | Cleber A. Ganzaroli^{1,2} | Wanderson R. H. Araujo^{1,2} |
Wesley P. Calixto^{1,2,3} 

¹Studies and Researches in Science and Technology Group (GCITE), Federal Institute of Goias (IFG), Goiânia, Brazil

²Electrical, Mechanical & Computer Engineering School (EMC), Federal University of Goias (UFG), Goiânia, Brazil

³Visualization, Simulation and Modeling (VSIM), Carleton University, Ottawa, Ontario, Canada

Correspondence

Alana S. Magalhaes, Studies and Researches in Science and Technology Group (GCITE), Federal Institute of Goias (IFG), Goiânia, Goias, Brazil.
Email: alana.magalhaes@ifg.edu.br

Wesley P. Calixto, Electrical, Mechanical & Computer Engineering School (EMC), Federal University of Goias (UFG), Goiânia, Brazil.
Email: wpcalixto@pq.cnpq.br

Funding information

Coordenação de Aperfeiçoamento de Pessoal de Nível Superior, Grant/Award Numbers: 1657377/2016-01, 88881.132192/2016-01, 88881.133454/2016-01, 88881.133765/2016-01; Brazilian Federal Agency for Support and Evaluation of Graduate Education; Foundation for Research Support of the State of Goias

Peer Review

The peer review history for this article is available at <https://publons.com/publon/10.1002/2050-7038.12365>.

Summary

This article proposes a comparison between mathematical modeling and experimental results of the electric interactions of a synchronous and an induction generator. The electric system is composed by a synchronous generator operating in parallel with the induction generator, both through a common bus, connected to nonlinear loads. Measurements are made at several points for different system configurations presenting the repowering effect. The analysis of the harmonic flow and the sensitivity of the system parameters are performed. To make predictions in the system, a validated computational model with experimental data is proposed. The results obtained comparing the mathematical modeling and experimental tests show the increase of the active power by the induction generator, as well as the circulation of harmonic currents in the common bus. The results obtained through the computational model present predictions of load unbalance and increase in the system harmonic distortions. The sensitivity analysis confirms the induction generator influences on the system harmonic flow.

KEYWORDS

induction generator, power generation, repowering, synchronous generator

1 | INTRODUCTION

The growing demand for electricity associated with increased production costs and concerns about environmental and socioeconomic issues, has led the world energy sector to expand power generation in the electricity systems, considering as an efficient utilization strategy the use of the existing sources, across by the repowering.¹ Repowering involves all activities that aim to achieve power and plant efficiency gains and occurs through the process of: (a) modification, (b) replacement, or (c) addition of equipment in the existing hydroelectric plant, in order to improve performance.

There are several researches developed with the purpose of repowering and improving the electric energy quality. According to Santos et al.,² an improvement in the winding of the synchronous generator is performed in order to increase the generated power. In the study, three calculation methods are performed to determine the synchronous generator field current. The results indicate an increase up to 50% in the generated power.

Gagliano et al.³ present a study to evaluate the economic and repowering prospects of the disused Catarrate plant in Petralia Sottana, interior of Sicily, Italy. The restructuring of the Catarrate plant contributes to the energy independence of the local community and preservation of historical industrial heritage. Its estimated annual production is ~220 MWh. Maldonado et al.¹ carry out studies at the Sodre plant in Guaratinguetá, São Paulo, Brazil. The results show that the repowering of hydroelectric plants, in particular the small hydroelectric power plant (SHP), can be a viable technical-economic and socio-environmental alternative to increase generation capacity. This is because the amortization time of invested capital is reduced due to the insertion of the carbon credits in the feasibility study.

The typical case of repowering is when the plant has idle power capacity in the turbine that is not used in generation. In these cases, when there is an increase in the volume of water in the reservoir, the generator (usually the synchronous generator) is working at maximum limit. Excessive water is wasted, not generating electricity. There are three options to repowering plants with these characteristics: (a) replacement of the synchronous generator by another larger synchronous generator, (b) addition of second synchronous generator, through double coupling to the turbine axis, (c) addition of second generator coupled to the turbine axis, but in this specific case, an induction generator.⁴⁻⁶

When the repowering is performed through replacing the synchronous generator by another larger synchronous generator or the addition of the second synchronous generator, it is necessary to consider the synchronization of the synchronous generator in the electric power system. This is a mandatory action, in order to prevent damage to the machines and disturbances in the electric system.⁷ Is presented in Pande and Kulkarni⁸ a smooth synchronizer technology with approaches in calculating the signal conditioner and estimation of angle-phase zero difference. The results show that smooth connection can be made between the electric power system and the synchronous generator.

Studies show repowering by induction generator as a viable technical-economic option.⁹ This approach presents low cost, less failure possibility, constructive simplicity, and less maintenance when compared to the synchronous generator. The inconvenience is the needing for external resources to compensate the reactives produced. In case of the lower power induction generator being connected to the common bus of the higher power synchronous generator, probable repowering case, the induction generator will have its reactives compensated by the synchronous generator. The coupling point between them will be without loss of power factor and control voltage be determined by the system.¹⁰⁻¹²

The demand for connection of small generators in the power grid has increased. Kundu¹³ is presented the technical requirements for parallel connection of generators in the Ontario/Canada hydroelectric distribution system. This study discusses some applications for connecting induction and synchronous generators in the power grid power system. The results indicate the requirements for connection of induction generators are less complex than for synchronous generators. Pham⁶ studies of load flow, short circuit, stability, coordination of protection devices, and protection requirements for the connection of induction generator in the electric system are presented. This work shows in the operation of synchronous machines in parallel it is necessary to use motorized thermomagnetic circuit breakers for the synchronization between the machines. The induction generator, in addition to low maintenance cost, does not require DC excitation and synchronization, reducing the cost with circuit breakers.

The synchronous generator connected to electrical power grid injects active and reactive power. However, the induction generator injects active power and needs to drain the systems reactive power, resulting in a low power factor. The study of Pongpornsup¹⁴ calculates the power flow using the AC Newton-Raphson method to analyze and verify the impact of the induction generator connection on the system. The focus of the work is the analysis of the voltage drop and total power loss occurred with the connection of the induction generator in the system without the power factor correction. Also informs that: (a) the connection position of the induction generator in the system, (b) the line parameters, and (c) the generation capacity affects the losses and the voltage drops of the system, requiring the induction generator power factor correction.

The study proposed by Reddy and Singh¹⁵ performs voltage and frequency control of parallel operation of synchronous and induction generators in micro hydro power plants. The synchronous generator has variable excitation under different load conditions while the induction generator has no excitation or speed control. This same study shows the connection of the induction generator in parallel with the synchronous is simpler than the connection between two synchronous generators in parallel. Any change in the reactive load is responded by synchronous generator to maintain the voltage at 1 pu. The induction generator does not respond to changing loads, always operating at full power. The

voltage and frequency control for parallel operation of synchronous generators and induction in micro hydro power plant can be realized by regulating device such as the static compensators (STATCOM).¹⁶⁻¹⁸

The repowering between synchronous and induction generators connected to the common bus in steady state, subject to nonlinear loads is presented in Magalhães et al.¹⁹ Magalhães presents the connection of synchronous generator and induction with the same power and of different powers, having the primary machine connected to the same bus of generators. Results show repowering of system and harmonic reduction in the common bus when the induction generator and synchronous generator are connected to the same bus. In interconnected power system (IPS) there are a number of high power synchronous generating units and nonlinear loads. The application of standards is recommended for limiting the harmonic content of the voltages in possible values of maintaining the acceptable quality of energy.²⁰

In repowering systems with parallel operation of synchronous and induction generators, the harmonic content must be monitored. Nailen²¹ analyzes the behavior of the grid connected to the induction generator, regarding overvoltage, frequency drift, harmonics, and power control. The results indicate that problems are rarely real and in most cases easily to be solvable. Liao et al²² analyze the effects of low frequency harmonics that originate in the rotor inverter of double fed induction generator. The harmonics are transferred to the stator and cause speed ripple, depending on the inertia and the operating condition of machine.

For a system as IPS, there is a need to know which parameter is most sensitive among the various parameters necessary for operation. Sensitivity analysis is the method capable to determine the most influential factors in the system being studied.²³ This method evaluates the variation of output response due to input parameters changes, measuring the effect of the input on a given output, and verifying the system response uncertainties caused by the input parameters uncertainties.²⁴ Sensitivity analysis can be performed using mathematical, statistical and graphical methods. Graphically, the impact caused on the output of system expresses the variations of input parameters. For k system parameters, $k - 1$ variables are held fixed at their base value while one of parameters is changed.²⁵

Santos et al² modifies the conductive and insulation materials to repower the system without the insertion of any other type of machine. Kundu¹³ presents the requirements and technical issues for parallel connection of synchronous and induction generators in the power grid, however it does not discuss the sensitivity of the system. Nailen²¹ analyzes the harmonics effect in power grid with presence of the induction generator, but does not analyze the flow of harmonics for each grid configuration, connecting the machines individually and together. The sensitivity analysis used in the experimental analysis of repowering was not found in the relevant literature.

Several studies are carried out with the aim of presenting the repowering of synchronous machines with induction machines. However, there are no studies regarding the connection of synchronous generator and induction with different powers, subject to the distortion of currents caused by nonlinear loads. This work has the objective of studying, comparing, and analyzing the results of system repowering, composed by: (a) synchronous generator, (b) induction generator operating in parallel with the synchronous generator, and (c) nonlinear loads.

This study is applied in subdimensioned hydroelectric power plants that have the option of adding the induction generator and can be repowering, taking advantage of the physical structures and reducing financial costs. Several hydroelectric plants have this feature, with idle power generation capacity because the reservoir water level is above the limit. The prediction of the system and the conduction of the simulation experiments will be accomplished through the construction of the computational model that represents the characteristics of the original system.

In systems with repowering through the induction machine, it is observed: (a) increase in the life of the main machine which is the synchronous machine, (b) reduction in the cost of acquisition and maintenance since the induction machine has a lower cost than the synchronous machine, and (c) easy to install due to the physical space since the volume of the induction machine compared to the synchronous machine, for the same power, is smaller. The innovation in this work is to evaluate the repowering performance using sensitivity analysis in experimental studies and to evaluate the harmonic flux and current distortions in the system in order to validate the induction generator as a harmonic attenuator when connected to the common bus.

This article contains the following structure: in Section 2 the theoretical basis for the mathematical modeling of the three-phase induction generator, three-phase synchronous generator, and the parallel association of the induction generator and the synchronous generator, besides the study of the sensitivity analysis. In Section 3 the proposed methodology for the experimental tests and for the connection of generators and nonlinear loads with the electric power grid is detailed. Also in Section 3 is presented the way in which the repowering, harmonic analysis, and sensitivity data will be analyzed. In Section 4 the experimental results are presented using the proposed methodology and in Section 5 the conclusions are found.

2 | THEORETICAL BACKGROUND

In order to perform the comparison between synchronous and induction machines, a mathematical analysis is presented of synchronous generator and induction generator in non-sinusoidal steady state. These analyzes made possible associate the synchronous and induction machines in a non-sinusoidal steady state, observing the behavior for each machine when subjected to harmonic components. The system modeling enable the possibility to test the insertion of nonlinear load and producing sensitivity analysis for each input system parameters.

2.1 | Three-phase induction generator

Figure 1 shows the electric circuit representing the non-sinusoidal steady-state induction machine, where X_E is the stator leakage reactance, \dot{E}_{ah} is the h order harmonic component of induced voltage in the stator phase a , due to the magnetic field produced by the sinusoidal spatial distribution of rotating magnetomotive force of h order, $fmm_{E0h} \cdot 2$ where \dot{I}_{ah} is stator a phase harmonic current, \dot{V}_{ah} is stator a phase harmonic voltage, and X'_{RB} is the blocked rotor reactance referred to the stator. The nonlinear load produces currents vary in a non-sinusoidal form, being composed by the fundamental and its harmonics. Considering the index h assuming odd values, probable condition produced by the nonlinear loads, the expression for all phases of the machine is given by:

$$\dot{V}_{hi} = \dot{Z}_{hi} \cdot \dot{I}_{hi} \quad (1)$$

where \dot{I}_{hi} is the harmonic current, \dot{V}_{hi} is the harmonic voltage, and \dot{Z}_{hi} is the stator harmonic impedance in the induction generator. The induction machine rotor electric circuit, in sinusoidal systems, has inductive reactance value much bigger than resistance value.^{26,27} In this way, the induction machine rotor behaves as an almost purely inductive element. For the stator electric circuit the resistance can also be neglected, since the ratio between the stator leakage reactance is much larger than resistance.²⁶ In the non-sinusoidal system, where the reactance values increase with increasing frequency, it is observed the relation between the reactance and the resistance increases even more.²⁶ Thus, the equivalent circuit presented in Figure 1 can be considered almost purely inductive and the impedance \dot{Z}_{hi} is given by:

$$\dot{Z}_{hi} = j \cdot h \cdot (X_E + k_R \cdot X'_{RB}) \quad (2)$$

Being $k_R \cdot X'_{RB}$ the resultant value between the parallel of the rotor leakage reactance X'_{RB} and the induction machine magnetization reactance. As the machine magnetization reactance is considerably greater than X'_{RB} , the parallel association is approximately X'_{RB} , so that k_R is ~ 1 . Since X'_{RB} can be considered approximately X_E and $k_R \rightarrow 1$, the following approximation can be made:

$$\dot{Z}_{hi} \cong j \cdot h \cdot 2X_E \quad (3)$$

Therefore, from (1), (2), and (3), leads to:

$$\dot{V}_{hi} \cong j \cdot h \cdot 2X_E \cdot \dot{I}_{hi} \quad (4)$$

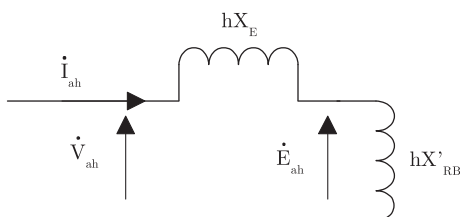


FIGURE 1 Induction machine representative electric circuit

Expression (4) expresses the non-sinusoidal steady-state induction generator can be represented by a purely inductive circuit because it is predominantly represented by inductive reactance.

2.2 | Three-phase synchronous generator

The stator harmonic voltage \dot{V}_{hS} for all the phases of the synchronous machine, adopting the usual nomenclature to represent the harmonic reactance, is given by (5), where r_E is the stator resistance per phase, X_S is the synchronous reactance at frequency ω , and X_{af} is the stator-rotor mutual at frequency ω .

$$\dot{V}_{hS} = (r_E + j \cdot h \cdot X_S) \cdot \dot{I}_{hS} + j \cdot \frac{h \cdot X_{af}}{2} \cdot \dot{I}_{f_h} \quad (5)$$

where \dot{I}_{hS} is the stator harmonic current in the synchronous generator and \dot{I}_{f_h} represents rotor current referred to the stator at frequency ω . The synchronous machine stator electric circuit, in sinusoidal systems, presents inductive reactance value much larger than the resistance value.^{26,27} The inductive reactance is proportional to the frequency, for non-sinusoidal state, while the h harmonic order increases, greater the reactance and greater the relation between the reactance and the circuit resistance.²⁶ In practice, it is possible consider $r_E \ll X_S$ ^{26,27} and the second portion of the expression (5) can be given by:

$$\dot{E}_h = j \cdot \frac{h \cdot X_{af}}{2} \cdot \dot{I}_{f_h} \quad (6)$$

Through (5) and (6), one has:

$$\dot{V}_{hS} \cong j \cdot h \cdot X_S \cdot \dot{I}_{hS} + \dot{E}_h \quad (7)$$

The expression (7) suggests the circuit of Figure 2, where \dot{E}_h is the h order harmonic component of the induced voltage in the synchronous machine stator.

Considering the rotor resistance small in the synchronous machine, which generally occurs, it can be considered.²⁶ Thus, the synchronous machine equivalent circuit can be represented by reactive and inductive component, whereas the electromagnetic effect between stator and rotor in the synchronous machine in the non-sinusoidal state is inductive in nature, similar to the induction machine.²⁶ Through the synchronous machine parameters analysis, it is observed the power flowing through the terminals \dot{E}_h is practically reactive inductive, suggesting, therefore, there is only inductive reactive impedance in the circuit relating \dot{V}_{hS} and \dot{I}_{hS} , which can be represented by $h \cdot X_S + \dot{E}_h$.

2.3 | Association between synchronous and induction machines

From the mathematical modeling of the synchronous and induction machines, it is possible to perform analysis by associating both machines in parallel, with the purpose of evaluating the behavior of the set when subjected to harmonic components. Therefore, by admitting one induction and one synchronous machines with same power, connected to the

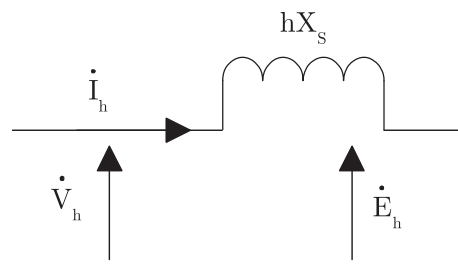


FIGURE 2 Cylindrical rotor synchronous machine equivalent circuit

same bus, it is possible to do the comparative analysis of the current harmonic components in both. The Figure 3 shows the synchronous and induction machines composed set.

The expression (4) of the induction machine and (7) of the synchronous machine can be rewritten using the representative circuit of the set shown in Figure 3. Since the induction and synchronous machines are connected in parallel on the same bus, the bus voltage will be the same for both, then $\dot{V}_{hs} = \dot{V}_{hi} = \dot{V}_h$ and therefore:

$$\dot{V}_h = j \cdot h \cdot (X_S + X) \cdot \dot{I}_{hs} = j \cdot h \cdot 2 \cdot X_E \cdot \dot{I}_{hi} \quad (8)$$

where $\dot{E}_h = j \cdot h \cdot X \cdot \dot{I}_{hs}$ and X is the equivalent reactance between the terminals of \dot{E}_h . Through algebraic manipulation in (8) give:

$$\frac{\dot{I}_{hi}}{\dot{I}_{hs}} = \frac{X_S + X}{2 \cdot X_E} \quad (9)$$

Assuming a threshold condition, where the value of X is insignificant compared to the value of a X_S^{26} and $X_S = 10 \cdot X_E^{26,27}$ the expression (9) can be rewritten:

$$\frac{\dot{I}_{hi}}{\dot{I}_{hs}} = 5 \quad (10)$$

The relation in (10) is due to the fact that X_S represents the armature reaction reactance plus the phase leakage reactance of the synchronous machine. Where X_E represents the leakage reactance per phase of the induction machine stator. The boundary condition imposed guarantees the inequality:

$$\dot{I}_{hi} > 5 \cdot \dot{I}_{hs} \quad (11)$$

From Equation (11) it is possible to observe in the same bus the harmonic currents will flow with greater intensity to the induction machine. This shows that besides the repowering due to the insertion of the induction machine, it is possible to use it as a means of absorbing the harmonic currents, attenuating the current harmonics of the synchronous machine. From this analysis it is possible to abstract that when the machine is only seen by the fundamental sinusoidal component, the energy flowing in the rotor is almost exclusively active, whereas when viewed by single harmonic component, the energy flowing in the rotor is almost entirely inductive. This allows to assume the intensities as irrelevant, or even the direction of the electromagnetic torque (motor or generator), to simulate the conditions of harmonic attenuation in synchronous machine.^{26,27}

The nonlinear equations of induction and synchronous machines can be linearized and applied over the operating point. The linear differential equations describe the dynamic behavior of the operating point and the system.²⁷ The

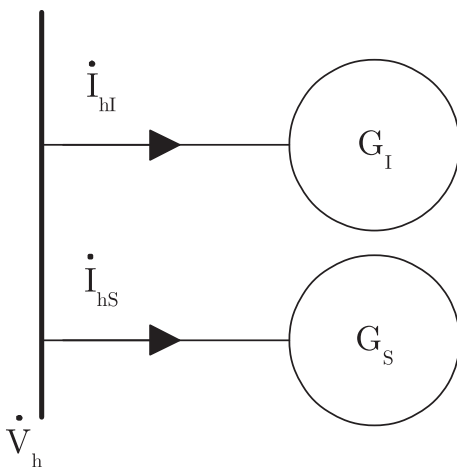


FIGURE 3 Set composed of synchronous generator and induction generator in parallel through a common bus

linearization of the machine equations, working around the operating point, results in linear equations in which one can analyze the own values of matrices and thus, justify the comparison of response speed for each type of machine.¹⁰

2.4 | System sensitivity analysis

The system sensitivity analysis evaluates the variation in the response of a given output variable due to changes in input parameter values. In other words, the sensitivity analysis measures what external interferences to the systems (input variables) can cause in the output values.²⁸ This is understood as the quest to quantify the relative contribution of each parameter in the system response.²³

The relationships between input and output are studied by means of experiments and simulations with the aim of indicating: (a) the most relevant parameter for analysis, seeking to reduce the uncertainties of the output (system robustness), (b) the least influential parameters, which can be maintained as constants, (c) parameters that make the output of the system more susceptible to changes (unstable), (d) the parameters of higher correlation with the output, and (e) the consequences of changes in parameter values when the system is running.^{23,29}

There are several methods to perform the sensitivity analysis of systems, which are classified according to the space exploration approach of inputs: (a) global or (b) local.³⁰ In the global sensitivity analysis all parameters are changed at the same time in of the study region.²⁴ In the local sensitivity analysis, one input parameter is varied at a time while the others remain fixed at the base value (or nominal).^{31,32} The base values of the input parameters correspond to: (a) optimal or optimized values obtained after the optimization process or (b) the best bet for inputs, defined by a specialist. The set of base values, $\alpha = (\alpha_1, \alpha_2, \dots, \alpha_n)$, is called the base case. So when the values of the input parameters correspond to the base case, the output $y = f(\alpha)$ and is called the base solution β .²⁵

The local sensitivity analysis can be performed in real system described by multiple inputs and multiple outputs from one-at-a-time measurements. The Figure 4 illustrates these measurements in multi-input and one-output systems, where $x = [x_1, x_2, \dots, x_n]$ is the matrix of input values that are varied one at a time and $y = [y_1, y_2, \dots, y_n]$ is the matrix with measured output values in the system. In this case, x_1 to x_n are vectors that assume values in the variation range of each parameter and y_1 to y_n are vectors with their respective outputs. The sensitivity analysis process is performed individually for each input until all input variables are analyzed.³³

Considering the methods of local sensitivity analysis, the analytical method proposed by Gomes³³ is based on one-at-a-time measurements and calculates the difference of the values of outputs with respect to the base solution β , as expressed in Equation (12). This method can be applied to systems whose parameters have different ranges of variation, even when the range only covers values close to the base value of the parameter.³⁴

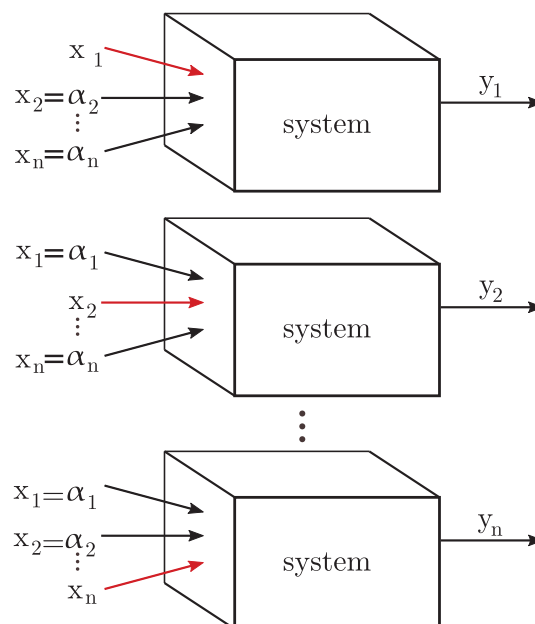


FIGURE 4 Sensitivity analysis one-at-a-time measures

In this method, the sensitivity index S_{x_i} is given by the relation between: (a) impact generated due to variations of parameter x_i and (b) impact resulting from all input variables, given by:

$$S_{x_i} = \frac{\frac{1}{k} \cdot \sum_{j=1}^k |y_{ij} - \beta|}{\sum_{i=1}^n \left(\frac{1}{k} \cdot \sum_{j=1}^k |y_{ij} - \beta| \right)} \quad (12)$$

where x_i is the parameter under review, n is the number of parameters, k is the number of one-at-a-time measurements per parameter, $y_{i,j}$ is the system output for j -th measurement of x_i , given by the function $y = f(x_1, x_2, \dots, x_n)$, and β the base solution.

3 | METHODOLOGY

The proposed methodology allows to performing experimental tests and analysis of the IPS from the workbench. The experimental tests are performed in two distinct workbenches, called B_1 and B_2 , composed of two generating units: a synchronous G_S and an induction G_I , connected in parallel, subjected to nonlinear loads. All elements connected to the same bus. Four metering devices are distributed in the system to analyze repowering and harmonic distortions. The workbench B_1 is composed of two generating units of the same power, in order to validate the presented mathematical modeling. The workbench B_2 is composed of a larger synchronous generating unit than the induction generating unit in order to validate the mathematical modeling for the specific case of repowering.

3.1 | Experimental setup

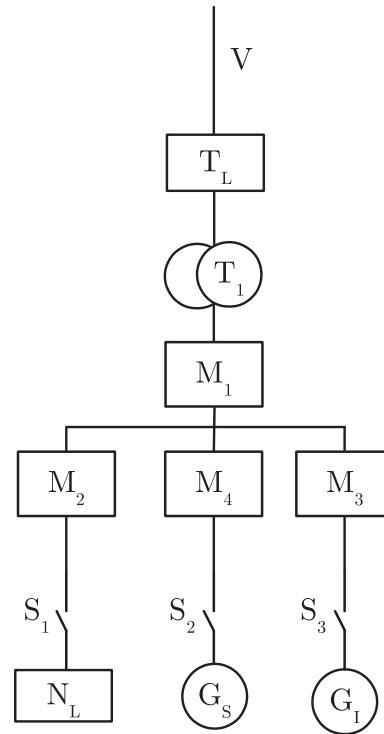
The experimental setup B_1 is composed by one synchronous generator G_S , one induction generator G_I , and nonlinear load N_L . The nonlinear load N_L is composed of three-phase fully controlled bridge rectifier (TPFCBR)³⁵ feeding sets of resistive load and a variable frequency drive (VFD). The primary machines used for G_S and G_I in workbench B_1 are DC motors. The workbench B_2 is composed by synchronous generator G_S , induction generator G_I and nonlinear load N_L . The nonlinear load of the B_2 workbench is composed of three-phase AC voltage controller (TPACVC)³⁵ feeding sets of resistive load. In the workbench B_2 , the primary machines used for the G_S is the diesel cycle engine and an induction motor with a VFD for the G_I . The nonlinear load is responsible for initially generating the harmonic distortions of the system current. Nailen²¹ states that the induction generator when connected to the power grid does not introduce harmonics into the system.

In the workbench B_1 and workbench B_2 tests are performed connecting the nonlinear load N_L to the common bus. In these tests it is aimed to obtain the harmonic distortions of the electric system shown in Figure 5, where T_L is the primary feeder, T_1 is the transformer, S_1, S_2, S_3 are keys for connection and $M_1, M_2, M_3,$ and M_4 are meters. The meter M_1 records data of the system electric parameters, such as power and harmonic values, in order to evaluate the increase of power generated and the system harmonic alterations. The meters $M_2, M_3,$ and M_4 record data of the system electric parameters that express the electric relations in the terminals of the nonlinear load, induction generator and synchronous generator, respectively. In this way it is possible to record the effects on the generation of electric power and changes on harmonic content with the system switching.

The measurements take place in three steps: (a) after the connection of the nonlinear load N_L , the synchronous generator G_S and the induction generator G_I are connected to the common bus, (b) after the measurements of the first step, the G_I is disconnected from the common bus and the effects of the exclusion of this generator on the system are measured, and (c) after the second step measurements, the G_S is disconnected from the bus and G_I is reconnected to the common bus. In this way, the generated power measurements and the changes in the harmonic content can be performed due to the insertion of the generators in the system for three different stages.

3.2 | Parallel connection of generators and nonlinear load with the power grid

There are some conditions necessary for the parallel operation of synchronous generators³⁶: (a) each generator must have the same line voltage, (b) generators connected in parallel must have the same phase sequence, (c) the phase

FIGURE 5 Illustration of the proposed interconnected power system

angles, in two phases, must be equal, and (d) the frequencies must be approximately equal, and for the machine entering the grid the frequency must be slightly higher. In (a) it is ensured that the voltages between the two generators, or between the generator and the grid, are equal. In condition (b) the sequence in which the phase voltages pass through peaks is ensured in the two generators it. In (c) it is ensured that in each phase the values of the voltage and angle are equal to every instant of time and in (d) it ensures that there is no reversal of power to avoid the generator being able to consume, instead of supplying power in given instant.

Failure to observe the synchronism can damage the synchronous generator due to the presence of high torques and currents, as well as causing problems in the power grid. Unlike the synchronous generator, the induction generator does not need to be synchronized with the voltage, frequency, and phase of the power grid to be connected.³⁶ For the coiled rotor induction motor as the primary machine, the frequency inverter and the three-phase rheostat are used for the drive, ensuring smoothing, and reduction of the starting current.

In case of connection in the power grid, the system has the property of maintaining constant the frequency and nominal voltage of the induction generator stator.³⁶ The induction generator is driven by the primary machine at a speed greater than the synchronous speed and slip is negative. From the synchronous speed, the induction machine will be in the generator condition, inserting power generated to the system. The reactive power required for excitation of induction generator can be provided by the system³⁶ or by the synchronous machine in the case of the parallel connection of a synchronous generator with induction generator.

For the experimental tests in workbench B_1 two kinds of nonlinear load were used. As stated previously, the nonlinear load N_{L1} is formed by TPFCBR which feeds resistive load and the nonlinear load N_{L2} is formed by a VFD. The nonlinear load used for the experimental workbench tests B_2 is formed by TPACVC feeding a resistive load set.

3.3 | Analysis of repowering, harmonic, and sensitivity data

The sets B_1 and B_2 , which are represented by the IPS shown in Figure 5, have the data recorded by energy analyzer at the measurement points where the outputs collected are: (a) active power P , (b) reactive power Q , (c) apparent power S , (d) power factor fp , (e) total harmonic distortion of voltage THD_V , and (f) total harmonic distortion of current THD_I .

The workbenches B_1 and B_2 allow to realize: (a) physical analysis between the synchronous generator and induction generator in non-sinusoidal steady state, (b) physical analysis in the association between synchronous generator and induction generator in a non-sinusoidal steady state, (c) verification of the repowering of the proposed IPS, and

(d) assessment of the harmonic content in the various measurement sites of the system. With these data it is possible to perform analyzes comparing the values obtained in the IPS with the limits defined by the standard IEEE STD 519-1992,²⁰ technical standard for voltage harmonics, where the restrictive value for THD_V is limited to 5% and current where the restrictive value for THD_I is limited from 4% to $h < 11$ and 2% to $11 < h < 17$. In this way, it is possible to verify the impact of voltage and current distortions in the IPS, subject to the nonlinear load, at each measurement point.

The IPS sensitivity analysis is performed only in the workbench B_2 through the data collected in M_1 . From the collected data it is possible to analyze the parameters: (a) active power P , (b) reactive power Q , (c) apparent power S , (d) power factor fp , (e) total harmonic distortion of voltage THD_V , and (f) total harmonic distortion of current THD_I . The purpose of collecting the data for sensitivity analysis is to connect all the keys of Figure 5 and vary the excitation voltage of the field of the synchronous generator, the mechanical power of the primary machine of the synchronous generator, the speed of the induction generator and the firing angle of the TPFCBR (nonlinear load). These variables were chosen because they were the IPS input variables.

In the experiments for sensitivity analysis, the value of the input variable is altered observing range of viable values, that is, not compromising the physical limit of the system. Although most methods of sensitivity analysis use the computational model of the system to obtain the outputs. It is possible to collect the desired data through experiments in the operating system, which is the proposed analysis in this work. The input variables chosen have different ranges of variation. Some of which operate only near the base value. In this case, the analytical method³³ of sensitivity analysis is indicated because it does not depend on the range of variation of each input variable.

3.3.1 | Model building and comparison between practical and simulated data

The computational model construction of the real IPS system, illustrated in Figure 5, is carried out in parts. First, the induction generator model is built, then the synchronous generator model and the nonlinear load model is built, and finally the electric power grid is modeled. All models are assembled and tested, giving rise to the full IPS computational model.

The proposed model to IPS is validated by comparing experimental data with simulated data. After validating the model, it is possible to perform computational tests and predictions. In the model, the output data is collected at the same measurement points M_1 , M_2 , M_3 , and M_4 used to measure the experimental data. The outputs measured in the simulation are the same as experimentally measured in the real system. With the experimental and simulated data, it is possible to perform: (a) comparison between model and real system, (b) sensitivity analysis, (c) verification of IPS repotentialization, (d) evaluation of harmonic content at measurement points M_1 , M_2 , M_3 , M_4 , and (e) predictions.

4 | RESULTS

From the proposed methodology it is possible to perform tests, obtaining the results that allow: (a) verify the repowering of the system, (b) validate the physical analysis of the synchronous and induction generators in the steady non-sinusoidal state, (c) validate the physical analysis of the association between the generators in the non-sinusoidal steady state, (d) to evaluate the harmonic content with the generators coupled to the system, and (e) to produce the sensitivity analyzes of the input parameters of the IPS.

4.1 | Definition of workbenches for experimental tests

The tests of the IPS shown in Figure 5, for the workbench B_1 , were performed with a system composed of two generating units: synchronous and inductive. Both units are in parallel by first feeding the TPFCBR constituting the nonlinear load N_{L1} and then TPFCBR and VFD constituting the nonlinear load N_{L2} . The Figure 6 shows the equipment used in the workbench B_1 .

The information about the components used in the workbench B_1 are set out in Table 1. The load N_{L1} , is the resistive load of 500 W, fed by TPFCBR. The load N_{L2} is composed of the resistive load of 300 W, fed by TPFCBR and the

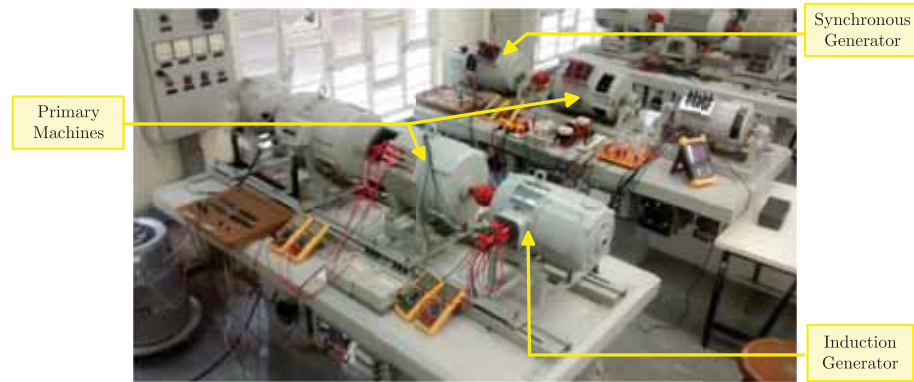
FIGURE 6 Workbench B_1 

TABLE 1 Acronyms and values of the components from IPS

Variables	Components	Values of used components
G_S	Synchronous generator (main generator)	2 kVA, 230 V three-phase, salient 4 poles, 60 Hz
G_I	Induction generator	2 kVA, 220 V three-phase, cage rotor 4 poles, 60 Hz
L_T	Primary feed	three-phase, 380 V, 60 Hz
T_1	Transformer	5 kW, 380/220 V, Δ/Y grounded
N_{L1}	Nonlinear load 1	500 W, three-phase, 380 V, 60 Hz
N_{L2}	Nonlinear load 2	500.4 W, three-phase, 380 V, 60 Hz

Abbreviation: IPS, interconnected power system.

induction motor of 2 kVA driven by frequency inverter with power of 200.4 W. As the primary machine of both generators, DC motors of 2 kW power were used.

The tests of the IPS shown in Figure 5, for the workbench B_2 , were performed with a system composed of one synchronous and one induction generating units. Both units are in parallel feeding the nonlinear load N_L consisting of TPFCBR to TPACVC which feeds resistive load with three-phase power of 14 kW. As G_S primary machine was used diesel cycle engine with 38.7 kW power and as G_I primary machine was used induction motor with 7.5 kW driven by frequency inverter with 9.2 kW of power. The Figure 7 shows the equipment used in the workbench B_2 , where the Figure 7A shows the induction generator and its primary machine and the Figure 7B shows the synchronous generator with the diesel cycle motor coupled.

The information about the components used on workbench B_2 are set out in Table 2 and the technical specifications for the meters M_1 , M_2 , M_3 , and M_4 are described in Table 3.

The workbench B_1 is composed of outworn machines and without preventive maintenance. The workbench B_2 is composed by the reconditioned set synchronous generator and diesel cycle engine and new set induction generator and induction motor.

4.2 | Repowering

The purpose of this test is obtaining the incremented power generated in the plant at measurement point M_1 for the workbenches B_1 and B_2 . The proposed configurations for the system are: (a) N_L where the nonlinear load is connected to system, (b) $G_S + G_I + N_L$ where the synchronous generator, the induction generator, and the nonlinear load are connected to the system, (c) $G_S + N_L$ where the synchronous generator and the nonlinear load are connected to the system, and (d) $G_I + N_L$ where the induction generator and the nonlinear load are connected to the system. For all repowering tests, the condition of generator operation was established to enable the $G_S + G_I + N_L$ configuration the power factor be greater than 80% and as close as possible to 100%.^{26,36}

The operating conditions of synchronous generator G_S and induction generator G_I in workbench repowering tests B_1 are arranged in Table 4. The values of active power, reactive power, apparent power, and power factor of G_S and G_I

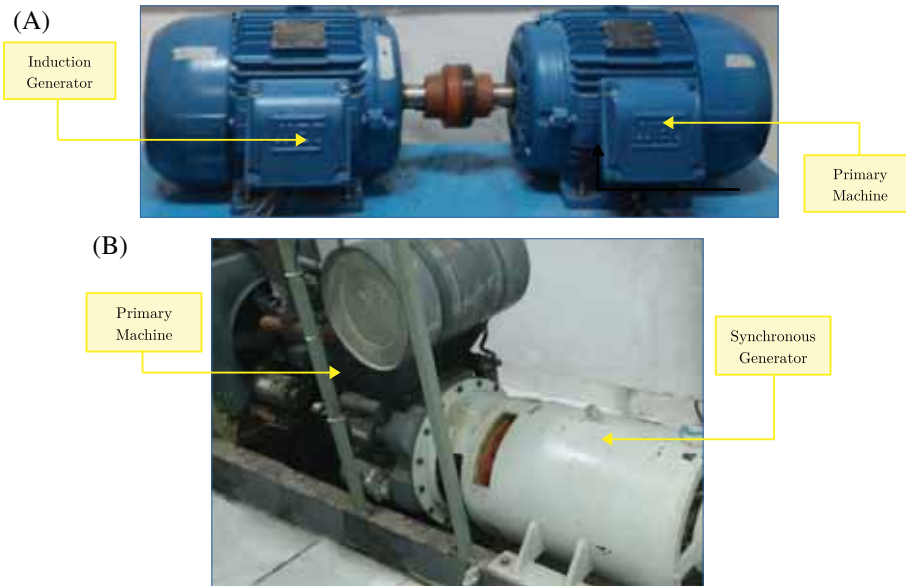


FIGURE 7 Workbench B_2 : A, induction generator and primary machine and B, synchronous generator with diesel engine

TABLE 2 Acronyms and values of the components from IPS

Variables	Components	Values of used components
G_S	Synchronous generator (main generator)	37 kVA, 380 V, fp 0.8 three-phase, salient 4 poles, 60 Hz
G_I	Induction generator	7.5 kVA, 380 V three-phase, cage rotor 4 poles, 60 Hz
L_T	Primary feed	three-phase, 13 800 V, 60 Hz
T_1	Transformer	750 kVA, 13 800/(380/220) V, Δ/Y grounded
N_L	Nonlinear load	14 kW three-phase, 380 V, 60 Hz

Abbreviation: IPS, interconnected power system.

Measurement	Measurement range		Accuracy
	Min	Max	
Frequency	40 Hz	70 Hz	\pm (0.01 Hz)
RMS voltage	1 V	1200 V	\pm (0.5% + 0.2 V)
RMS current	1 A	1200 A	\pm (0.5% + 0.2 A)
Active power	5 mW	7800 kW	\pm (1%) $\cos \Phi \geq 0.8$
Reactive power	5 mVAr	7800 kVAr	\pm (1%) $\sin \Phi \geq 0.5$
Apparent power	5 mVA	7800 kVA	\pm (1%)

TABLE 3 Accuracy specifications

were obtained at the measurement points M_4 and M_3 , respectively, for loads N_{L1} and N_{L2} . Tables 5 and 6 provide the data of active power, reactive power, apparent power, and power factor at measuring point M_1 for all configurations proposed with nonlinear loads N_{L1} and N_{L2} , respectively.

In Tables 5 and 6, it is noted the power factor in M_1 in $G_S + G_I + N_L$ configuration is 0.92 for N_{L1} and 0.80 for N_{L2} . For nonlinear load N_{L1} , in N_L configuration, the grid is providing active power of 500 W. With the connection of the synchronous generator and induction generator, in $G_S + G_I + N_L$ configuration, the grid will receive active power of 1644 W. Disconnecting G_I , going to $G_S + N_L$ configuration, the grid will receive active power of 681 W with N_{L1} . In comparison with $G_S + N_L$ configuration, commonly found in the plants, it is observed that with the insertion of G_I , the system repowering occurs at 141.41% in active power generated.

TABLE 4 Workbench B_1 : active power, reactive power, apparent power, and power factor of G_S and G_I to N_{L1} and N_{L2}

Operation	N_{L1}		N_{L2}	
	G_S	G_I	G_S	G_I
P (W)	-1085	-1007	-1116	-1530
Q (V Ar)	-3595	3783	-3995	4197
S (V A)	3767	3964	4146	4473
fp	0.291	0.256	0.269	0.343

TABLE 5 Workbench B_1 : active power, reactive power, apparent power, and power factor in M_1 to N_{L1}

Configuration	N_{L1}			
	P (W)	Q (V Ar)	S (V A)	fp
N_L	500	174.9	531.3	0.943
$G_S + G_I + N_L$	-1644	818	1865	0.92
$G_S + N_L$	-681	-3379	3454	0.2
$G_I + N_L$	-514	3949	3995	0.133

TABLE 6 Workbench B_1 : active power, reactive power, apparent power, and power factor in M_1 to N_{L2}

Configuration	N_{L2}			
	P (W)	Q (V Ar)	S (V A)	fp
N_L	500	500	700	0.718
$G_S + G_I + N_L$	-2100	1300	2697	0.80
$G_S + N_L$	-700	-3300	3400	0.224
$G_I + N_L$	-900	4800	4900	0.19

For the nonlinear load N_{L2} , in N_L configuration, the grid is providing active power of 500 W. In $G_S + G_I + N_L$ configuration, the grid will receive active power of 2100 W. Disconnecting G_I , the grid will receive 700 W. The repowering of the system is observed with the insertion of G_I , at 200% compared to $G_S + N_L$ configuration, increasing the active power generated.

The operating conditions of the G_S and G_I for the workbench B_2 tests are shown in Table 7 for inductive G_S , configuration where synchronous generator is receiving reactive power of grid. Measurements of the active power values, reactive power, apparent power, and power factor were performed at points M_4 and M_3 .

The Table 8 provides data of active power, reactive power, apparent power, and power factor for the measurement point M_1 in various configurations proposed for the nonlinear load N_L for inductive G_S . The excitation of the synchronous generator was adjusted to obtain a power factor of M_1 in $G_S + G_I + N_L$ configuration as close to unit.

In the N_L configuration, Table 8, the grid provides active power of 2547 W. In the $G_S + G_I + N_L$ configuration, Table 8, the grid receives active power of 23 820 W. In this case, it has the nonlinear load receiving 2547 W, the synchronous generator providing 22 684 W and the induction generator providing 3636 W, Table 7. This totals 23 820 W of power supplied. Disconnecting G_I , the synchronous generator, in the $G_S + N_L$ configuration, Table 7, provides active power of 22 684 W. The synchronous generator feeds the nonlinear load and supplies the grid with remaining generated power. For this case, the grid will receive active power of 20 043 W. It is observed, with the insertion of the induction generator, the system repowering has increased of 18.84% in the active power generated, compared to the $G_S + N_L$ configuration. It is also observed the power factor measured in M_1 , in $G_S + G_I + N_L$ configuration is 0.86. This occurs because the power factor of the synchronous generator is 0.80.

The operating conditions of the G_S and G_I for workbench B_2 repowering tests, to capacitive G_S , configuration where the synchronous generator is supplying reactive power to the system, are arranged in Table 9. Measurements of the active power values, reactive power, apparent power, and power factor were performed at measuring points M_4 and M_3 .

Table 10 provides the data of active power, reactive power, apparent power, and power factor for the measurement point M_1 in the various configurations proposed for the nonlinear load N_L with capacitive G_S . The excitation of the synchronous generator was adjusted to obtain a power factor of M_1 , in $G_S + G_I + N_L$ configuration as close to unit.

Operation	P (W)	Q (V Ar)	S (V A)	fp
G_S	-22 684	5657	23 396	0.969
G_I	-3636	4502	5795	0.629

TABLE 7 Workbench B_2 : active power, reactive power, apparent power, and power factor with inductive G_S and G_I to N_L

Configuration	P (W)	Q (V Ar)	S (V A)	fp
N_L	2547	3602	6710	0.559
$G_S + G_I + N_L$	-23 820	13 157	27 688	0.860
$G_S + N_L$	-20 043	9014	22 553	0.888
$G_I + N_L$	-1105	8090	9601	0.147

TABLE 8 Workbench B_2 : active power, reactive power, apparent power, and power factor in M_1 with inductive G_S and N_L

Operation	P (W)	Q (V Ar)	S (V A)	fp
G_S	-22 444	-12 080	25 508	0.88
G_I	-3135	1338	5972	0.525

TABLE 9 Workbench B_2 : active power, reactive power, apparent power, and power factor for capacitive G_S and G_I to N_L

Configuration	P (W)	Q (V Ar)	S (V A)	fp
N_L	2474	2960	5517	0.425
$G_S + G_I + N_L$	-23 786	-4795	24 635	0.965
$G_S + N_L$	-20 127	-9072	22 476	0.895
$G_I + N_L$	-1921	7012	7881	0.243

TABLE 10 Workbench B_2 : active power, reactive power, apparent power, and power factor in M_1 with capacitive G_S and N_L

In the N_L configuration, the grid is providing active power of 2474 W, Table 10. In $G_S + G_I + N_L$ configuration, the grid is receiving active power of 23 786 W, Table 10. In this case, one has the nonlinear load receiving 2474 W, the synchronous generator providing 22 444 W, and the induction generator providing 3135 W, Table 9. The system is providing 23 786 W, Table 10. With the withdrawal of G_I , in the $G_S + N_L$ configuration provides active power of 22 444 W, Table 9. In this case the grid will receive active power of 20 127 W, Table 10. It is observed that with the insertion of the induction generator, the system repowering has increased of 18.18% in the active power generated in comparison with $G_S + N_L$ configuration. It is also observed that the power factor in M_1 , in $G_S + G_I + N_L$ configuration, is 0.96.

When G_S is capacitive and provides reactive to G_I , in M_1 it is observed that the value of the power factor is close to 0.96 for $G_S + G_I + N_L$ configuration, as Table 10. In the case of inductive G_S , the power factor value is 0.86 for $G_S + G_I + N_L$ configuration, as Table 8. The G_S can operate inductive or capacitive and in the case of repowering with induction machine. It is usual that it operates as capacitive, providing the reactive to G_I . In this mode of operation, the G_S has a lower power factor and still supplies the reactive demand of G_I , when connected in parallel.

In the workbenches B_1 and B_2 the repowering of the system was obtained. In the case of parallelism of generators with the same power, in workbench B_1 , repowering is observed from 141.41% to N_{L1} and from 200.00% to N_{L2} . For generators of different powers, where G_S is 4.93 times greater than G_I , the repowering is observed from 18.84% to inductive G_S and from 18.18% to capacitive G_S .

This is the typical case of repowering, where it presents G_S as the main generator and G_I as the secondary generator connected in parallel on the same bus. For the tests performed in workbench B_1 , the primary machines are of greater power than the generators, allowing more active power produced. The power contribution generated by G_I , in tests carried out in workbench B_2 , becomes less expressive because they present machines of different powers.

4.3 | Harmonics analysis

In the same tests performed to measure repowering, using the same operating conditions as in Tables 4, 7, and 9, the data of the harmonic distortions were collected. For all harmonic analysis tests the condition of operation of generators

was established so that in $G_S + G_I + N_L$ configuration the power factor is greater than 0.80 and close to unit.^{26,36} The measured results of total harmonic distortions of current THD_I at measurement points M_1 , M_2 , M_3 , and M_4 , were collected by observing the total harmonic distortions of voltage THD_V within the limits set up in IEEE STD 519-1992.²⁰ The values established in the standard for voltage harmonics varies according to the voltage class at point to be measured. In workbench B_1 and workbench B_2 , where measurements were carried out in the voltage of 220 and 380 V, respectively, the limit of the total harmonic distortion of voltage THD_V is 5.0% and the threshold of the individual harmonic distortion of voltage DHI_V is 3.0%. The limits for the individual harmonic distortion of current DHI_I is from 4% to $h < 11$ and 2% to $11 < h < 17$.

The values of THD_V and THD_I for workbench B_1 at measurement points M_1 , M_3 , and M_4 with nonlinear loads N_{L1} and N_{L2} are shown in Tables 11 and 12, respectively. These values are for all proposed configurations.

At the point of measurement M_1 and using as nonlinear load N_{L1} , Table 11, it is noted that the value THD_V reduces to 1.5% in the $G_S + G_I + N_L$ configuration, increases from 1.9% to 2.1% in $G_S + N_L$ configuration and reduces to 1.7% in $G_I + N_L$ configuration. It is noted that the value of THD_I in N_L configuration is 23.1%. In $G_S + G_I + N_L$ configuration the value of THD_I is reduced to 15.4%. In $G_I + N_L$ configuration the value reduces to 5.6% and in $G_S + N_L$ configuration the value reduces to 4.6%. This indicates that both the synchronous generator and the induction generator reduces the THD_I in the IPS. It should be noted that the condition of operation of the generators has been established so that in $G_S + G_I + N_L$ configuration has power factor as close as possible to unit. In this way, the generators are operating in a parallelism condition, with G_S providing reactive power to G_I and with a view to improving power factor.

In the $G_S + G_I + N_L$ configuration, the THD_I value in M_3 is 2.8% and in M_4 is 1.5%, with repowering of machines of the same power the harmonic content is greater in the terminals of G_I than in the G_S , indicating that the G_I behaves as a preferred path for harmonic currents. In Table 12, using as load the nonlinear N_{L2} , at the measurement point M_1 with N_L configuration, it is observed the value of THD_V reducing from 1.8% to 1.6% in the $G_S + G_I + N_L$ configuration and reduces from 1.8% to 1.7% for $G_S + N_L$ and $G_I + N_L$ configurations. The value of THD_I is 81.9% to N_{L2} configuration and for the configuration $G_S + G_I + N_L$ the value of THD_I reduces to 28.7%. In $G_S + N_L$ configuration value reduces to 14.3% and in $G_I + N_L$ configuration value reduces to 12.7%. These reductions demonstrate that both the G_S and G_I produce reduction in THD_V and THD_I in IPS. The measured values of THD_V and THD_I in workbench B_1 using N_{L2} in points of measurements M_3 and M_4 , are values close to values obtained in the tests of workbench B_1 using N_{L1} and therefore, the considerations are the same.

In the configuration $G_S + G_I + N_L$, for both non-loads N_{L1} and N_{L2} , it observes a reduction of THD_V and THD_I in M_1 , indicating that, with repowering, there is a reduction of the harmonic content. In $G_S + N_L$ configuration the reduction of THD_V and THD_I in M_1 is also observed. Indicating that the G_S operating in parallelism, also reduces the harmonic content of system. It is important to note that in all tests the G_S operated in parallel condition, providing reactive to induction generator. In the configuration $G_I + N_L$ the reduction of THD_V and THD_I in M_1 is also observed, indicating that the induction generator reduces harmonic content of system.

TABLE 11 Workbench B_1 : THD_V (%) and THD_I (%) to M_1 , M_3 , and M_4 with N_{L1}

Configuration	THD_V			THD_I		
	M_1	M_3	M_4	M_1	M_3	M_4
N_L	1.9	-	-	23.1	-	-
$G_S + G_I + N_L$	1.5	1.5	1.4	15.4	2.8	1.5
$G_S + N_L$	2.1	-	2.0	4.6	-	1.8
$G_I + N_L$	1.7	1.7	-	5.6	3.3	-

TABLE 12 Workbench B_1 : THD_V (%) and THD_I (%) to M_1 , M_3 , and M_4 with N_{L2}

Configuration	THD_V			THD_I		
	M_1	M_3	M_4	M_1	M_3	M_4
N_L	1.8	-	-	81.9	-	-
$G_S + G_I + N_L$	1.6	1.4	1.4	28.7	3.0	1.3
$G_S + N_L$	1.7	-	1.8	14.3	-	1.8
$G_I + N_L$	1.7	1.8	-	12.7	3.3	-

Figure 8 shows the current waveforms for all configurations adopted in the inductive G_S tests for the workbench B_2 . Figure 8A shows the current waveform for the N_L configuration and Figure 8B shows the current waveform for $G_S + G_I + N_L$ configuration. Figure 8C shows current waveform for $G_S + N_L$ configuration and Figure 8D presents the waveform for the $G_I + N_L$ configuration.

Figure 9 shows the current waveforms for all configurations adopted in capacitive G_S tests for workbench B_2 . Figure 9A shows the current waveform for N_L configuration and Figure 9B shows the current waveform for $G_S + G_I + N_L$ configuration. Figure 9C shows the current waveform for $G_S + N_L$ configuration and Figure 9D shows the waveform for $G_I + N_L$ configuration.

For the workbench B_2 , the values of THD_V and THD_I , arranged in Table 13 and Table 14, at the measurement points M_1 , M_2 , M_3 , and M_4 with inductive and capacitive G_S , respectively. At the M_1 measurement point to inductive G_S with N_L configuration, it is observed that value of THD_V reduces from 1.6% to 1.4% in $G_S + G_I + N_L$ configuration, and THD_I reduces from 114.2% to 18.9% in $G_S + G_I + N_L$ configuration. The reductions of THD_V and THD_I in M_1 , for the $G_S + N_L$ and $G_I + N_L$ configurations, are the result of greater active power flow that causes harmonics to be diluted in relation between active power and apparent power.

In $G_S + G_I + N_L$ configuration the value of THD_I is 3.0% in M_3 and 2.9% in M_4 , with repowering of machines of different powers, with G_S greater than G_I . It has that harmonic content is greater in terminals of G_I than in G_S , again indicating that the G_I behaves as the preferred path for harmonic currents.

At the point of measurement M_1 for the capacitive G_S and N_L configuration, Table 14, it is observed that value of THD_V reduces from 1.8% to 1.6% in $G_S + G_I + N_L$ configuration, and the THD_I value for N_L configuration in M_1 is 104.5% and in $G_S + G_I + N_L$ configuration the value reduces to 17.7%. The values obtained for THD_I at measurements points M_3 and M_4 , with capacitive G_S , are similar to test with inductive G_S , so the analysis is the same.

It should be noted that condition of operation of generators has been established so that in $G_S + G_I + N_L$ configuration has power factor close to one. For the inductive G_S , it has that G_S and G_I receive reactive power of grid and for capacitive G_S , G_S provides reactive power to G_I , in order to improve power factor of the set. In the $G_S + G_I + N_L$ configuration the reduction of THD_V and THD_I in M_1 to inductive and capacitive G_S , indicating that with the repotentialization there is reduction of harmonic content.

In $G_S + G_I + N_L$ configuration, for the workbench B_1 , where generators are of same power, it is observed that there are more harmonics at connection bus of G_I than in connection bus of G_S . For N_{L1} the THD_I in G_I is 2.8% and G_S is 1.5% and to N_{L2} the THD_I in G_I is 3.0% and G_S is 1.3%. For workbench B_2 , there is a small difference in harmonics at connection bus of G_I when compared to harmonics at connection bus of G_S , being greater in connection bus of G_I . For

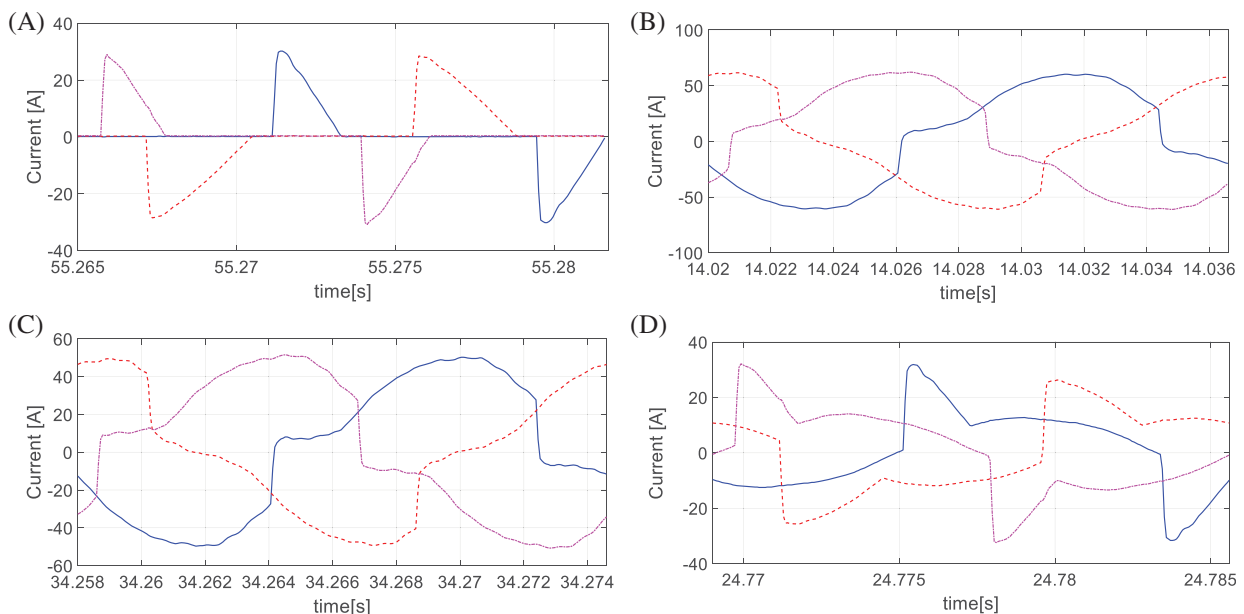


FIGURE 8 Current waveforms measured in workbench B_2 in M_1 with inductive G_S : A, with N_L connected; B, with $G_S + G_I + N_L$ connected; C, with $G_S + N_L$ connected; and D, with $G_I + N_L$ connected

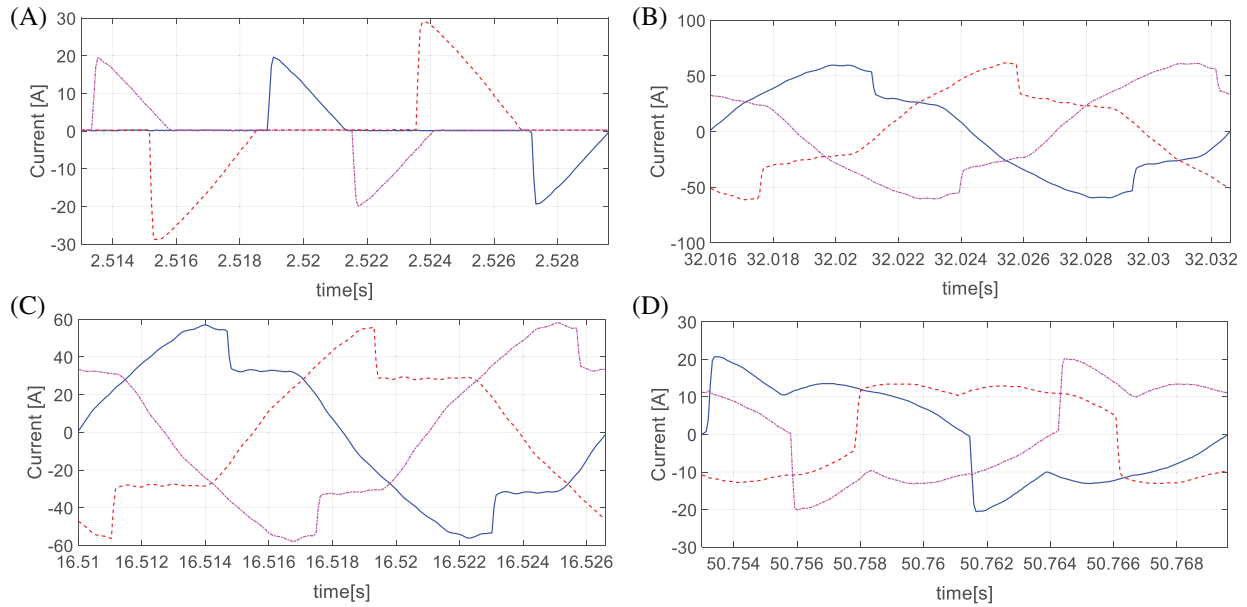


FIGURE 9 Current waveforms measured in workbench B_2 in M_1 with capacitive G_S : A, with N_L connected; B, with $G_S + G_I + N_L$ connected; C, with $G_S + N_L$ connected; D, with $G_I + N_L$ connected

TABLE 13 Workbench B_2 : THD_V (%) and THD_I (%) to M_1, M_2, M_3 , and M_4 with N_L and inductive G_S

Configuration	THD_V				THD_I			
	M_1	M_2	M_3	M_4	M_1	M_2	M_3	M_4
N_L	1.6	1.6	-	-	114.2	114.3	-	-
$G_S + G_I + N_L$	1.4	1.5	1.5	1.4	18.9	112.1	3.0	2.9
$G_S + N_L$	1.4	1.4	-	1.4	23.2	112.1	-	2.8
$G_I + N_L$	1.5	1.5	1.6	-	59.7	113.5	3.2	-

TABLE 14 Workbench B_2 : THD_V (%) e THD_I (%) to M_1, M_2, M_3 , and M_4 with N_L and capacitive G_S

Configuration	THD_V				THD_I			
	M_1	M_2	M_3	M_4	M_1	M_2	M_3	M_4
N_L	1.8	2.0	-	-	104.5	105.2	-	-
$G_S + G_I + N_L$	1.6	1.7	1.7	1.6	17.7	105.9	3.9	3.5
$G_S + N_L$	1.7	1.7	-	1.7	19.2	106	-	3.8
$G_I + N_L$	1.8	1.8	1.8	-	41.6	105.7	4.1	-

inductive G_S the THD_I in G_I is 3.0% and in G_S is 2.9% and for capacitive G_S the THD_I in G_I is 3.9% and G_S is 3.5%. It is observed that for two generators of same size, the preferred path for harmonics is G_I . When G_S is much larger than G_I , proportionally, there will still be more harmonics in G_I than G_S .

It can be seen from Tables 11, 12, 13, and 14 that the THD_I value is significantly high in the N_L configuration. Nonlinear loads are responsible for system current distortion in the practical experiments. In other configurations, it is possible to notice changes in THD_I value because both G_I and G_S change the harmonic flow of the system.

The workbench B_2 is composed of G_S and G_I with different powers. Thus, absolute values of current measured in points of M_1, M_2, M_3 , and M_4 for the $N_L, G_S + G_I + N_L, G_S + N_L$, and $G_I + N_L$ configurations, making possible to perform a comparative analysis between two generators. Tables 15 and 16 have the harmonic current values I_h in absolute value [A] with inductive and capacitive G_S , respectively, considering phase a of the system.

In Table 15, it is noted that the value of I_h in M_1 is 7.8A for the N_L configuration. In the $G_S + G_I + N_L$ configuration value reduces to 7.6A, which represents $\sim 2.5\%$ of attenuation of the harmonic currents in M_1 . In the $G_S + N_L$

Configuration	I_h (A)			
	M_1	M_2	M_3	M_4
N_L	7.8	-	-	-
$G_S + G_I + N_L$	7.6	7.8	0.3	1.0
$G_S + N_L$	7.5	7.8	-	1.0
$G_I + N_L$	7.7	7.7	0.3	-

TABLE 15 Workbench B_2 : I_h to $M_1, M_2, M_3,$ and M_4 with N_L and inductive G_S , phase a

Configuration	I_h (A)			
	M_1	M_2	M_3	M_4
N_L	5.0	-	-	-
$G_S + G_I + N_L$	5.7	4.8	0.3	1.4
$G_S + N_L$	5.7	4.8	-	1.4
$G_I + N_L$	4.8	4.9	0.3	-

TABLE 16 Workbench B_2 : I_h to $M_1, M_2, M_3,$ and M_4 with N_L and capacitive G_S , phase a

configuration the value reduces to 7.5A which represents $\sim 3.8\%$ due to the G_S , in the $G_I + N_L$ configuration the value reduces to 7.7A representing $\sim 1.2\%$ due to G_I .

In Table 16, it is noted that the value of I_h in M_1 is 5.0A for N_L configuration. In $G_S + G_I + N_L$ and $G_S + N_L$ configurations, the value increases to 5.7A, representing $\sim 14.0\%$ increase from I_h to M_1 . In $G_I + N_L$ configuration the value reduces to 4.8A, which represents 4.0% attenuation of I_h , indicating G_S increases the harmonic currents in M_1 . In all tests the harmonic current flow was constant for G_I in the $G_S + G_I + N_L$ and $G_I + N_L$ configurations and to G_S in the $G_S + N_L$ and $G_S + G_I + N_L$ configurations.

By analyzing Tables 15 and 16, it is seen that the G_I decreases the I_h of bus subjected to nonlinear load. The G_S reduces the I_h of bus subject to the nonlinear load when it is subexcited, that is, when it operates inductively. On the flip side, the synchronous generator increases the harmonic currents of bus under nonlinear load when it is overexcited, when it operates capacitively.

4.3.1 | Analysis of individual harmonic distortions of current

***The Table 17 shows the most significant individual harmonic distortions of current DHI_1 measured in M_1 with N_{L1} connected in workbench B_1 , in configuration N_L , where upper fifth order h^5 with 19.0% and eleventh order h^{11} with 9.0%. THD_V and THD_I after entering G_I and G_S , with nonlinear load connected to system, $G_S + G_I + N_L$ configuration, was 1.5% and 15.4%, respectively. Comparing with N_L configuration, the THD_I reduced from 23.1% to 15.4% and the most significant DHI_1 were the third order h^3 with a reduction of 7.6% to 6.1% and fifth order h^5 with increase from 19.0% to 19.2%, the values of other harmonics are set in Table 18.

Table 19 sets values of individual harmonics for the N_L configuration with inductive G_S . All individual harmonics for N_L were significant with values above 9.9%. Table 20 sets values of individual harmonics for $G_S + G_I + N_L$ configuration with inductive G_S . The most significant individual harmonics were third order h^3 with reduction from 87.5% to 16.7%, the fifth order h^5 with a reduction from 66.3% to 10.0% and seventh order h^7 with reduction from 43.0% to 5.1%. The objective of this test was to maintain power factor closest to one in M_1 to make comparisons of values obtained in other tests. The individual harmonic distortions of current DHI_1 measured in M_1 was greater for N_L configuration. For $G_S + G_I + N_L$ configuration there was a reduction of DHI_1 .

Table 21 sets individual harmonic values for the N_L configuration. All individual harmonics were significant with values above 9.6% to N_L . Table 22 has values of the individual harmonics for $G_S + G_I + N_L$ configuration with capacitive G_S . The most significant individual harmonics were third order h^3 with reduction from 83.0% to 18.8%, the fifth order h^5 with reduction from 56.0% to 11.2% and seventh order h^7 with reduction from 31.0% to 4.4%. The purpose of this test was to maintain the power factor close to one in M_1 to analyze harmonic reduction in relation to N_L and

TABLE 17 Workbench B_1 : DHI_1 in M_1 with N_{L1}

THD_V	1.9%		
THD_I	23.1%		
Harmonic	AB	BC	CA
60 Hz (Fnd)	100.0%	100.0%	100.0%
180 Hz (h^3)	6.9%	0.3%	7.6%
300 Hz (h^5)	19.0%	16.1%	17.8%
420 Hz (h^7)	8.8%	7.4%	4.3%
540 Hz (h^9)	0.5%	0.5%	5.8%
660 Hz (h^{11})	5.1%	5.7%	9.0%
780 Hz (h^{13})	3.0%	3.2%	5.9%
900 Hz (h^{15})	3.3%	0.4%	3.8%

TABLE 18 Workbench B_1 : DHI_1 in M_1 with $G_S + G_I + N_{L1}$

THD_V	1.5%		
THD_I	15.4%		
Harmonic	AB	BC	CA
60 Hz (Fnd)	100.0%	100.0%	100.0%
180 Hz (h^3)	5.3%	6.1%	5.4%
300 Hz (h^5)	19.2%	2.0%	10.3%
420 Hz (h^7)	1.6%	1.2%	1.1%
540 Hz (h^9)	2.2%	0.0%	2.0%
660 Hz (h^{11})	2.9%	1.1%	2.0%
780 Hz (h^{13})	2.8%	1.1%	2.1%
900 Hz (h^{15})	1.3%	0.1%	0.8%

TABLE 19 Workbench B_2 : THD_I in M_1 to inductive G_S with N_L connected

THD_V	1.6%		
THD_I	114.2%		
Harmonic	AB	BC	CA
60 Hz (Fnd)	100.0%	100.0%	100.0%
180 Hz (h^3)	86.4%	70.2%	87.5%
300 Hz (h^5)	63.9%	33.2%	66.3%
420 Hz (h^7)	39.9%	20.0%	43.0%
540 Hz (h^9)	23.7%	19.0%	25.3%
660 Hz (h^{11})	20.3%	12.8%	19.5%
780 Hz (h^{13})	19.9%	11.5%	18.9%
900 Hz (h^{15})	16.4%	9.9%	16.1%

$G_S + G_I + N_L$ configuration. A significant reduction is observed in the individual harmonic distortions of current DHI_1 measured in M_1 for the $G_S + G_I + N_L$ configuration in relation to N_L configuration.

4.3.2 | Voltage and current distortions

For workbench B_1 , Tables 11 and 12, the values of THD_V do not exceed 2.1%, for N_{L1} and N_{L2} , falling within the 5% limit set by the IEEE STD 519-1992 standard.²⁰ By observing Tables 17 and 18, at measuring point M_1 with N_{L1} , 81% of

THD_V	1.4%		
THD_I	18.9%		
Harmonic	AB	BC	CA
60 Hz (F_{nd})	100.0%	100.0%	100.0%
180 Hz (h^3)	12.2%	16.7%	12.1%
300 Hz (h^5)	9.6%	10.0%	9.3%
420 Hz (h^7)	5.1%	4.6%	4.9%
540 Hz (h^9)	3.2%	3.8%	3.0%
660 Hz (h^{11})	3.2%	2.7%	2.9%
780 Hz (h^{13})	2.8%	2.5%	2.7%
900 Hz (h^{15})	2.2%	2.1%	2.1%

TABLE 20 Workbench B_2 : THD_I in M_1 with $G_S + G_I + N_L$ connected and inductive G_S

THD_V	1.8%		
THD_I	104.5%		
Harmonic	AB	BC	CA
60 Hz (F_{nd})	100.0%	100.0%	100.0%
180 Hz (h^3)	83.0%	70.0%	82.0%
300 Hz (h^5)	56.0%	32.0%	54.0%
420 Hz (h^7)	31.0%	20.0%	30.0%
540 Hz (h^9)	21.0%	19.0%	21.0%
660 Hz (h^{11})	21.0%	13.0%	20.0%
780 Hz (h^{13})	17.0%	12.0%	16.0%
900 Hz (h^{15})	13.0%	9.6%	11.0%

TABLE 21 Workbench B_2 : THD_I in M_1 to capacitive G_S with N_L connected

THD_V	1.6%		
THD_I	17.7%		
Harmonic	AB	BC	CA
60 Hz (F_{nd})	100.0%	100.0%	100.0%
180 Hz (h^3)	8.9%	18.8%	7.8%
300 Hz (h^5)	9.8%	11.2%	9.7%
420 Hz (h^7)	3.9%	4.4%	3.4%
540 Hz (h^9)	2.2%	4.2%	2.0%
660 Hz (h^{11})	1.7%	3.7%	1.9%
780 Hz (h^{13})	2.1%	2.9%	2.0%
900 Hz (h^{15})	1.5%	2.4%	1.2%

TABLE 22 Workbench B_2 : THD_I in M_1 with $G_S + G_I + N_L$ connected and capacitive G_S

the individual harmonic distortion values of current DHI_I , exceed the limits established in standard and in $G_S + G_I + N_{L1}$ configuration 33% of DHI_I values exceed established standard limits.

For workbench B_2 , Tables 13 and 14, the values of THD_V do not exceed 1.6% to N_L with inductive G_S and 2.0% to N_L with capacitive G_S . Tables 19 and 20, at the measuring point M_1 with inductive G_S , in the N_L configuration 100% of values obtained of DHI_I exceeds limits set in standard and in $G_S + G_I + N_{L1}$ configuration 71% of values obtained of DHI_I exceed limits of standard. Observing Tables 21 and 22, at measurement point M_1 , with capacitive G_S , in N_L configuration 100% of the values obtained of DHI_I exceed limits established in standard. In $G_S + G_I + N_{L1}$ configuration 57% of values obtained of DHI_I exceed limits of standard.

The expression (10) establishes relationship between the harmonic current of the induction generator \dot{I}_{hI} and harmonic current of synchronous generator \dot{I}_{hS} to machines of same power. For machines with different powers, the relation can be rewritten as:

$$\frac{\dot{I}_{hI}}{\dot{I}_{hS}} = \frac{X_S}{2 \cdot X_E} \quad (13)$$

With generator reactance values obtained in manufacturers catalog, it is possible to calculate relationship between synchronous generator synchronous reactance X_S and induction generator stator leakage reactance X_E . Figure 10 shows the relation $\frac{X_S}{2 \cdot X_E}$ when varying power of generators.

It is observed in Figure 10 that when the powers are equal value in ordinates axis is ~ 5 , corroborating with expression (10). It is observed that with power increasing of induction machine the ratio given in Equation (13) increases. Thus, it can be stated that when one has G_I of greater power it will absorb harmonic of the IPS. With the increase in power of G_S the ratio given in Equation (13) decreases. Thus, it can be stated that when we have the G_S of greater power when compared to the G_I , the harmonic flow that will be absorbed by G_I will be smaller proportionally.

The electric equipment operating in the harmonic frequencies have greater losses and greater possibility of insulation failures, when compared with electric equipment that operate in the fundamental frequency. The use of frequency inverters contributes to the increase of harmonic contents in electric network.³⁷ With repowering using the proposed methodology, lifetime of synchronous generator increases while lifetime of induction generator decreases. However, the economic value of induction generator is $\sim 40\%$ lower than synchronous generator. In addition, the volume of the induction generator is $\sim 85\%$ less than the volume of synchronous generator. The induction machine presents greater ease and economy in maintenance and exchange. In this way, in addition to repowering system, the lifetime of the synchronous machine is increased.

4.4 | Model validation and comparison between practical and simulated data

The simulations were performed using the computational model represented by Figure 5 for the B_2 workbench, whose parameters are described in Table 2. Model validation is given by comparing experimental and simulated data. For model validation, the output variables were used: (a) active power P , (b) reactive power Q , and (c) apparent power S . Comparison between experimental and simulated data for the complete IPS system is illustrated in Figure 11.

The average errors calculated between the experimental and simulated values are: (a) 8.7% for P , (b) 2.3% for Q , and (c) 3.9% for S . It is observed that through these results the computational model is representative of the real system illustrated in Figure 5.

4.4.1 | Sensitivity analysis

From the validated model, sensitivity analysis was performed using experimental data and simulated data collected on the M_1 meter. The input parameters analyzed are: (a) nonlinear load rectifier firing angle, θ , (b) mechanical power of G_S primary machine, P_{MEC} , (c) speed of induction generator, ω_{GI} , and (d) field excitation voltage of synchronous

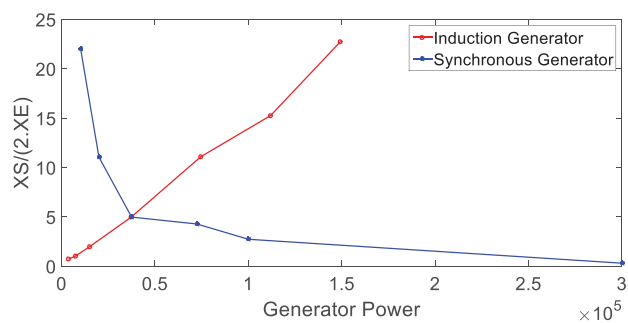


FIGURE 10 Ratio $\frac{X_S}{2 \cdot X_E}$ varying the power of the generator

generator, V_f . The output parameters observed are: (a) active power P , (b) reactive power Q , (c) apparent power S , (d) power factor fp , (e) total distortion voltage harmonic THD_V , and (f) total current harmonic distortion THD_I .

To perform sensitivity analysis in IPS, you need to set the base value of the input parameters θ , P_{MEC} , ω_{GI} , V_f , and their respective ranges within the feasible operating space. These values are arranged in Table 23.³³

Table 23 shows that the variation range of the parameters for the simulation is greater than the variation range for the experimental tests. The P_{MEC} variable, for example, had a range from -40.59% to 0% for the experimental test and for computer simulation the range increased to -47.00% to 96.08% . Thus, in the computational environment one can analyze the system in other operating points, which were not possible in experimental tests.

From the base value, the parameters are varied one-at-a-time within the viable IPS operating space and each output value is recorded. The experimental data collected are presented in Figure 12, where the abscissa axis represents the variations made in the parameters from the base value (crossing point of all curves) and the ordinate axis represents each output analyzed. The outputs analyzed were: (a) Figure 12A active power P , (b) Figure 12B reactive power Q , (c) Figure 12C apparent power S , (d) Figure 12D power factor fp , (e) Figure 12E total voltage harmonic distortion THD_V , and (f) Figure 12F total current harmonic distortion THD_I . Experimental and simulated data were applied in Equation (12) to quantify the sensitivity of each parameter and Table 24 sets out the sensitization indices found.

When analyzing Table 24, the sensitivity of 55% for P_{MEC} and 31% for θ in the experimental data is observed and 45% for P_{MEC} and 41% for θ in the simulated data, indicating that when parsing the active power output P , these are the two most sensitive variables. The V_f variable has approximately zero sensitivity for the P output and can be set as constant in this case. These results are consistent with practical knowledge indicating that the variation in P can be obtained by increasing the generated power of G_S or by changing the load consumption θ or by increasing the generated power of G_I . For the reactive power output Q , the most sensitive variables are P_{MEC} with 64% and V_f with 28% for experimental data and P_{MEC} with 56% and V_f with 37% for the simulated data. The ω_{GI} variable could be considered constant when analyzing the output Q , because in practice, when you want to change the reactive G_S , you change the excitement by varying the field.

For the power factor fp the situation is similar to the reactive power Q , with the variable ω_{GI} close to zero. For the apparent power output S , no variable can be fixed, that is, considered constant. For the output total harmonic distortion current THD_I the variable ω_{GI} could be considered constant, however, the most sensitive variable using experimentally

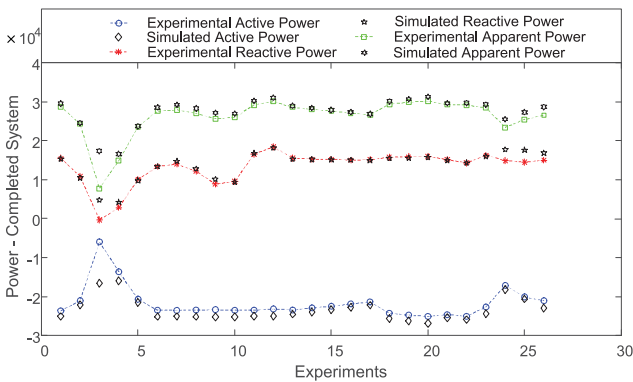


FIGURE 11 Comparison between simulated and experimental for the complete system

TABLE 23 Base value and ranges of variation for IPS input parameters

Parameter	Base value	Experimental		Simulated	
		Range ^a	Variation (%)	Range ^a	Variation (%)
θ	132.83°	(80.85140.5)	(-39.13 5.77)	(2180)	(-98.49 35.51)
P_{MEC}	18.87 kV A	(11.21 18.87)	(-40.59 0)	(10.00 37.00)	(-47.00 96.08)
ω_{GI}	1840 rpm	(1815 1855)	(-1.36 0.81)	(1800 1860)	(-2.17 1.09)
V_f	41.5 V	(38.8 48)	(-6.51 15.66)	(28.92 71.77)	(-30.31 74.70)

Abbreviation: IPS, interconnected power system.

^aThe units are the same as the base value.

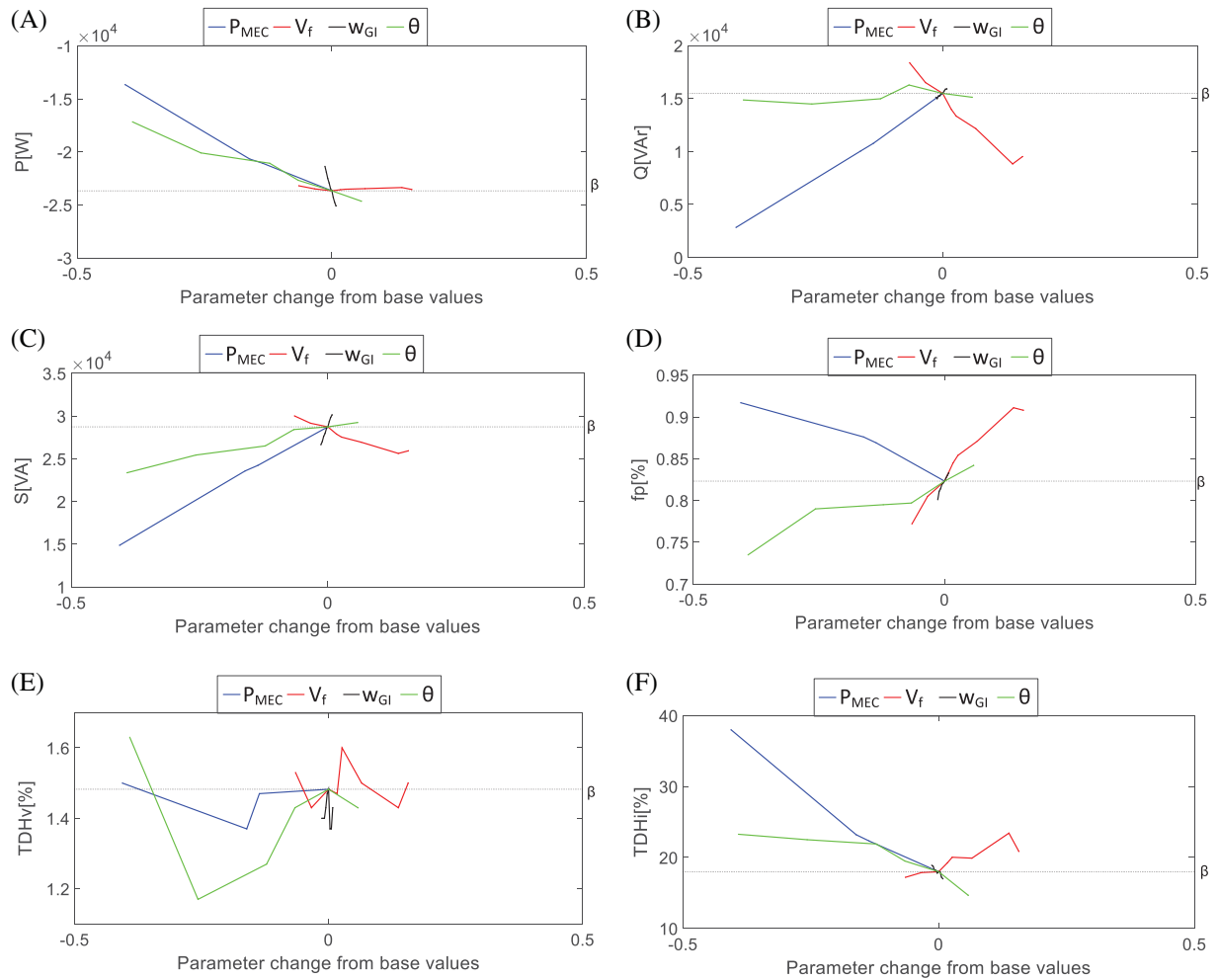


FIGURE 12 Experimental sensitivity curves given by one-at-a-time measurements for the outputs: A, active power; B, reactive power; C, apparent power; D, power factor; E, THD_V and F, THD_I

TABLE 24 Sensitivity indexes of IPS parameters

Output	Experimental				Simulated			
	$S_{P_{MEC}}$	S_{V_f}	$S_{w_{GI}}$	S_{θ}	$S_{P_{MEC}}$	S_{V_f}	$S_{w_{GI}}$	S_{θ}
P	0.55	0.02	0.12	0.31	0.45	0.01	0.13	0.41
Q	0.64	0.28	0.02	0.06	0.56	0.37	0.01	0.06
S	0.60	0.13	0.09	0.18	0.61	0.12	0.08	0.19
fp	0.40	0.30	0.06	0.24	0.32	0.27	0.05	0.36
THD_V	0.15	0.14	0.23	0.48	0.59	0.10	0.10	0.21
THD_I	0.61	0.13	0.04	0.22	0.34	0.11	0.07	0.48
Average	0.49	0.17	0.09	0.25	0.48	0.16	0.07	0.29

Abbreviation: IPS, interconnected power system.

collected data is P_{MEC} and the variable the most sensitive using simulated data is θ . This change in the most sensitive variable between model and experimental occurs due to different operating ranges (between experiment and model, see Table 23). In the model, when using the same range as the experimental one, the most sensitive variable becomes the P_{MEC} variable. This indicates that the operating range influences the value of the sensitivity indexes.

On average, for the workbench B_2 experiments, it can be stated that of the four parameters analyzed, P_{MEC} has the highest sensitivity with $\sim 48.5\%$, θ is the second most sensitive with $\sim 27\%$, V_f is the third most sensitive with $\sim 16.5\%$, and

ω_{G_I} is the least sensitive with ~8%. The sensitivity index shown in Table 24 can be used at the time of system parameter adjustments, indicating which parameter should be changed first and how much can be changed in the value of each parameter. The sensitivity index can also be used in the optimization process when adjusting the model to the system.

4.5 | Model analysis and predictions for the repowered system

With the validated model it is possible to make predictions for IPS. In these predictions two irregular conditions were proposed. First, there is load unbalance, where the total three-phase power is changed from 14 to 19.7 kW. In the second simulation, the distortion value was doubled when compared to the initial distortion value.

4.5.1 | Load unbalance

To perform load unbalance prediction, the computational simulation of Figure 5 was used. In this simulation the input values were considered the same as those established for the inductive G_S experimental tests. Measurements of active power, reactive power, apparent power, and power factor were taken at M_4 and M_3 . To perform the unbalance was reduced the resistance value of one of the phases by 41.3%. The G_S and G_I operating conditions for this simulation are laid out in Table 25.

For the experimental test, the operating points obtained are arranged in Table 7. In the simulation with the unbalanced system, the operating points provided in Table 25 are obtained. Note that there was a change from 2.04% to 20.24% on the trading point values of G_I and G_S when unbalanced. Thus, it is noted that with the load changes generating the unbalance in one of the phases, the generators modify the amount of power generated in order to power the system connected to it.

A prediction was made for four system configurations in order to verify the influence of load unbalance in each configuration. The settings are the same as those used in the experimental data, arranged in Table 8. Table 26 displays the active power, reactive power, apparent power, and power factor data at measurement point M_1 for all four configurations and with the system unbalanced. Table 26 shows the increase in active power, reactive power and apparent power in the N_L configuration, due to load unbalance. Note that even with the unbalanced system, with the addition of G_I in the $G_S + G_I + N_L$ configuration, there is system repowering.

The prediction for the four configurations was made in order to verify the harmonic behavior of the system due to the unbalance, was made. The THD_V and THD_I values obtained for the unbalanced system are arranged in Table 27, at measurement points M_1 , M_2 , M_3 , and M_4 .

With load unbalance there are changes from 5.52% to 73.33% in the values of THD_I , when compared to the values obtained in the experimental data, arranged in Table 13. In Table 27, in the $G_S + G_I + N_L$ setting THD_I is 5.2% on M_3 and 4.4% on M_4 , this indicates that even in the case of load unbalance the harmonic content is higher in the G_I terminals than in the G_S terminals, reaffirming that G_I behaves as the preferred path for harmonic currents.

Operation	P (W)	Q (V Ar)	S (V A)	fp
G_S	-22 221	5325	22 885	0.971
G_I	-4372	4995	6646	0.659

TABLE 25 Prediction at operating point M_4 and M_3 due to load unbalance

Configuration	P (W)	Q (V Ar)	S (V A)	fp
N_L	5682	4978	7821	0.612
$G_S + G_I + N_L$	-21 215	15 403	26 601	0.792
$G_S + N_L$	-16 933	10 444	20 388	0.818
$G_I + N_L$	1744	10 331	11 166	0.087

TABLE 26 Powers and power factor predictions in M_1 due to load unbalance

4.5.2 | Increased electric grid harmonic distortion

To predict the increase in the electric grid harmonic distortion, the same input values defined for the G_S capacitive experimental tests were used. Measurements of active power, reactive power, apparent power, and power factor were taken at M_4 and M_3 . The power grid was modeled along with the G_S and G_I machines and the N_L load, completing the IPS model. To make changes in distortions, simply modify some variables in the grid model. In this simulation the value of the distortions were increased by 100%. The operating conditions of G_S and G_I in the model are laid out in Table 28.

Table 9 arranges the operating points of the generators for the system without increasing distortion and Table 28 arranges the operating points for the system with the distortion increased by 100%. When the system is subjected to increased distortion, there are changes from 1.98% to 279.67% on the trading point values of G_I and G_S . The increase in reactive power generated is 36.38% for G_I and 279.67% for G_S . Thus, it can be said that with the increase of distortions in the grid, the generators G_S and G_I absorb the excess reactive power in IPS.

A prediction was made in the four configurations increasing the harmonic distortions of the electric grid, in order to verify the system repotentialization. The settings used are shown in Table 10. Table 29 provides the active power, reactive power, apparent power, and power factor data at measurement point M_1 for the four distortion-incrementing configurations. With the increase of distortions and the addition of G_I in the $G_S + G_I + N_L$ configuration, there is the system repowering.

In order to verify the system harmonic behavior due to the increase of the grid harmonic distortions, the prediction was performed. The THD_V and THD_I values obtained for the system at the measurement points M_1 , M_2 , M_3 , and M_4 , subject to the network distortion increment are arranged in the Table 30.

TABLE 27 Prediction of voltage and current distortions due to load unbalance

Configuration	THD_V				THD_I			
	M_1	M_2	M_3	M_4	M_1	M_2	M_3	M_4
N_L	2.0	2.0	-	-	90.7	90.7	-	-
$G_S + G_I + N_L$	2.0	2.0	2.0	2.0	25.9	90.7	5.2	4.4
$G_S + N_L$	2.0	2.0	-	2.0	33.8	90.7	-	4.4
$G_I + N_L$	2.0	2.0	2.0	-	63.0	90.7	5.2	-

TABLE 28 Prediction at operating point in M_4 and M_3 due to increased distortion

Operation	P (W)	Q (V Ar)	S (V A)	fp
G_S	-24 753	-7685	26 014	0.952
G_I	-4375	5080	6731	0.654

TABLE 29 Powers and power factor prediction in M_1 due to increased distortion

Configuration	P (W)	Q (V Ar)	S (V A)	fp
N_L	1249	2023	2425	0.621
$G_S + G_I + N_L$	-27 821	-729	27 908	0.997
$G_S + N_L$	-23 581	-5617	24 296	0.971
$G_I + N_L$	-3080	7158	8030	0.401

TABLE 30 Prediction of voltage and current distortions due to increased distortion

Configuration	THD_V				THD_I			
	M_1	M_2	M_3	M_4	M_1	M_2	M_3	M_4
N_L	3.6	3.6	-	-	117.2	117.2	-	-
$G_S + G_I + N_L$	3.6	3.6	3.6	3.6	12.1	117.2	10.0	7.3
$G_S + N_L$	3.6	3.6	-	3.6	13.3	117.2	-	7.3
$G_I + N_L$	3.6	3.6	3.6	-	42.4	117.2	10.0	-

In Table 30, in the $G_S + G_I + N_L$ setting THD_1 is 24.8% at M_3 (G_I meter) and 18.7% at M_4 (G_S meter). Even with the significant increase in distortion the harmonic content is higher in the G_I terminals than in the G_S terminals. With the increase in power grid distortion there were changes from 1.92% to 156.41% in the values of THD_1 between the experimental data provided in Table 14 and the simulated/predicted for all the settings.

5 | CONCLUSION

This work is mostly integrated by workbench tests. It is concluded that induction generator in connection with synchronous generator connected to nonlinear load has the capacity, besides increasing the power generated, to attenuate the harmonic distortions of current and voltage, in common bus.

The tests of workbench B_1 , with G_I and G_S of the same power, reaffirm the proposal of use of inductions G_I for repowering and can also attenuate the harmonics of main generators of plants. Assuming the G_I in parallel as the G_S , the G_I will have total harmonic distortion of current greater in its terminals. The results for workbench B_2 , with $G_I < G_S$, also reaffirms the proposal of using induction generators for repowering and use as harmonic attenuator in main generators of plants. By associating G_I in parallel as G_S of greater power, it is estimated that G_I will have total harmonic distortion of current proportionally greater in its terminals. Thus, all tests performed in workbench B_1 and workbench B_2 reduced the harmonic content in terminals of main generator of IPS.

The tests of workbench B_2 demonstrate that G_S in a steady non-sinusoidal state can work as a harmonic generator when it supplies reactive power to the grid (capacitive) and as harmonic absorber when it absorbs reactive power from the grid (inductive). For configuration $G_S + G_I + N_L$ it is observed that absolute value of current in M_4 is greater than in M_3 . Considering G_S with power 4.93 times greater than G_I , it can be stated that the harmonic current value proportional to the power of machine is more significant in M_3 .

The induction generator, besides presenting low cost, greater robustness, constructive simplicity, low maintenance, and smaller dimension, when compared with synchronous generator of same power, are able to repowering the system. The results show reductions in harmonic distortion in bus, both with connection of synchronous generator and connecting an induction generator. The results indicate the induction generator provides a preferential path for harmonic currents even when the two generators produce or consume equivalent and proportional reactive powers. The synchronous generator presents different behaviors when it is subexcited or overexcited, reducing or increasing, respectively, the harmonic currents of bus subjected to nonlinear load. In sensitivity analysis, the synchronous generator current and nonlinear load firing angle are the most sensitive parameters independent of synchronous machine producing or consuming reactive power. The analytical sensitivity analysis method expresses coherent sensitivity index values even with variables containing ranges of variation within the different viable space. The results also confirm the total harmonic distortion of current is sensitive to induction generator since it affects the system harmonic content. Model predictions have shown that G_I is the preferred path for harmonic currents and that the system is repowered, even when the system is subject to load unbalance or increased grid harmonic distortion. The innovative results for the scientific community are the indication that G_I is responsible for repowering in addition to attenuating the content of harmonic components. This provides increased synchronous machine life and reduces the financial costs of maintenance and purchase. The sensitivity analysis of the system allows to know the most sensitive parameters and thus monitors them to prevent unwanted system shutdown.

ACKNOWLEDGEMENTS

The authors would like to thank National Council for Scientific and Technological Development (CNPq), Foundation for Research Support of the State of Goias (FAPEG) and Brazilian Federal Agency for Support and Evaluation of Graduate Education (CAPES) for scholarships: 88881.133765/2016-01, 88881.133454/2016-01, 88881.132192/2016-01, and 1657377/2016-01.

CONFLICT OF INTEREST

The authors declare no potential conflict of interest.

AUTHOR CONTRIBUTIONS

A.S.M. and W.P.C. developed the mathematical modeling. A.S.M., V.M.G., C.A.G., and W.P.C. developed the methodology. A.S.M., A.H.F.S., J.S.B., M.R.C.R., C.A.G., and A.J.A. applied the methodology and conducted the experiment in

loco. A.S.M., A.J.A, G.A.W., and W.P.C. analyzed and treated the data collected. All authors analyzed the results and A.S.M., A.H.F.S., and G.A.W. collaborated writing the manuscript.

DATA ACCESSIBILITY

Some or all data, models, or code generated or used during the study are available from the corresponding author by request as: all experimental data collected from workbench B1 and workbench B2.

NOMENCLATURE

X'_{RB}	blocked rotor reactance referred to the stator
\dot{E}_{ah}	h order harmonic component of induced voltage in the stator phase a
\dot{E}_h	h order harmonic component of the induced voltage in the synchronous machine stator
\dot{I}_{hl}	harmonic current
\dot{V}_{hl}	harmonic voltage
$k_R \cdot X'_{RB}$	resultant value between the parallel of the rotor leakage reactance X'_{RB} and the induction machine magnetization reactance
\dot{I}_{fh}	rotor current referred to the stator at frequency ω
\dot{I}_{ah}	stator a phase harmonic current
\dot{V}_{ah}	stator a phase harmonic voltage
\dot{I}_{hS}	stator harmonic current in the synchronous generator
\dot{Z}_{hl}	stator harmonic impedance in the induction generator
\dot{V}_{hS}	stator harmonic voltage for all the phases of the synchronous machine
B_1, B_2	experimental setups
DC	direct current
DHI_1	individual harmonic distortions of current
fmm_{Eoh}	magnetic field produced by the sinusoidal spatial distribution of rotating magnetomotive force of h order
fp	power factor
G_1	induction generator
G_S	synchronous generator
h	order
IPS	interconnected power system
k	number of one-at-a-time measurements per parameter
M_1, M_2, M_3, M_4	meters
n	number of parameters
N_L	nonlinear load
P	active power
P_{MEC}	mechanical power of G_S primary machine
Q	reactive power
r_E	stator resistance per phase
S	apparent power
S_1, S_2, S_3	keys for connection
SHP	small hydroelectric power plant
STATCOM	static compensators
T_1	transformer
THD_1	total harmonic distortion of current
THD_V	total harmonic distortion of voltage
T_L	primary feeder
TPACVC	three-phase AC voltage controller
TPFCBR	three-phase fully controlled bridge rectifier
VFD	variable frequency drive
X	equivalent reactance between the terminals of \dot{E}_h

X_{af}	stator-rotor mutual at frequency ω
X_E	stator leakage reactance
x_i	parameter under review
X_S	synchronous reactance at frequency ω
$y_{i,j}$	system output for j -th measurement of x_i , given by the function $y = f(x_1, x_2, \dots, x_n)$
β	base solution
θ	nonlinear load rectifier firing angle
ω	frequency of the synchronous machine
ω_{GI}	speed of induction generator
V_f	field excitation voltage of synchronous generator

ORCID

Alana S. Magalhaes  <https://orcid.org/0000-0003-2027-1783>

Wesley P. Calixto  <https://orcid.org/0000-0002-1928-4432>

REFERENCES

- Maldonado OA, Panunzio PA, Silva DF, Silveiras JL. Technique-economical viability of repowering of small hydroelectric power plant considering the social insert and environmental preservation. *Renew Energ Power Qual J.* 2006;4:1-5.
- Santos SPY, Delbone E, Carvalho EF, Martins LN. Repower and evaluation of new power of synchronous generators. *Am J Appl Sci.* 2011;8:594-602.
- Gaglianoa A, Tinab GM, NOceraa F, Pataniaa F. Technical and economic perspective for repowering of micro hydro power plants: a case study of an early XX century power plant. *Bologna PowerTech Conf.* 2014;62:512-521.
- Magalhães AS, Junior LCA, Matias CA, et al. Repowering of a synchronous generation plant by induction generator. Paper presented at: IEEE Congreso Chileno de Ingeniería Eléctrica, Electrónica, Tecnologías de la Información y Comunicaciones (IEEE CHILECON 2015), 2015; Santiago.
- Magalhães AS, Moraes PHF, Silva AHF, Gomes PHG, Alves AJ, Calixto WP. Parallel operation repowering of synchronous and induction generator. Paper presented at: 16th International Conference on Environment and Electrical Engineering (EEEIC), 2016; Florence, Italy
- Pham KD. Cogeneration application: interconnection of induction generators with public electric utility. Paper presented at: Rural Electric Power Conference - REPC, 1991
- Paz MCR, Obadowski VN, Oliveira MO, et al. Synchronization method for synchronous generator based on UPFC. *PowerTech.* 2013;1:1-5.
- Pande AS, Kulkarni NG. Advanced technique for soft synchronizer in CHP cogeneration. *Int J Adv Eng Technol.* 2015;7:1760-1766.
- Chapallaz JM, Ghali JD, Eichenberger P, Fischer G. Manual on motors used as generators. *MHPG Series*, Vol. 10, Friedr. Vieweg & Sohn Verlagsgesellschaft mbH, Germany
- Singh M, Singh SP, Singh B, Pandey AS, Dixit R, Mittal N. Stand alone power generation by 3 ϕ asynchronous generator: a comprehensive survey. Paper presented at: International Conference on Power, Control and Embedded Systems, 2012.
- Singh GK. Self-excited induction generator research - a survey. *Electr Power Syst Res.* 2004;69:107-114.
- Wang L, Tsao C-C. Performance analyses of a three-phase induction generator connected to a utility grid. Paper presented at: Power Engineering Society Winter Meeting; 2001.
- Kundu D. Technical requirements to connect parallel generators to the ontario hydro distribution electricity system. *IEEE Trans Energ Conv.* 1992;7:8-14.
- Pongpornsup V. Impacts of non-utility induction generator to distribution network. *IEEE Transm Distrib Conf Exhib.* 2002;2:1352-1356.
- Reddy PJ, Singh SP. Voltage and frequency control of parallel operated synchronous and induction generators in micro hydro scheme. *Comput Power Energ Inform Comm.* 2014;1:124-129.
- Gawande SP, Porate KB, Thakre KL, Bodhe GL. Synchronization of synchronous generator and induction generator for voltage & frequency stability using STATCOM. Paper presented at: Third International Conference on Emerging Trends in Engineering and Technology; 2010.
- Tamrakar I, Shilpakar LB, Fernandes BG, Nilsen R. Voltage and frequency control of parallel operated synchronous generator and induction generator with STATCOM in micro hydro scheme. *Gener Transm Distrib.* 2007;1:743-750.
- Freitas W, Asada E, Morelato A, Xu W. Dynamic improvement of induction generator connected to distribution system using a DSTATCOM. *Power Syst Technol.* 2002;1:173-177.
- Magalhães AS, Moraes PHF, Silva AHF, Gomes PHG, Alves AJ, Calixto WP. Reconditioning in synchronous operation with one parallel induction generator. *Trans Environ Elect Eng.* 2016;1:66.
- IEEE Std 519-1992. IEEE Recommended Practices and Requirements for Harmonic Control in Electrical Power Systems. New York; 1993.
- Nailen RL. Spooks on the power line? Induction generators and the public utility. *IEEE Trans Ind Appl.* 1982;IA-18(6):608-615.

22. Liao Y, Ran L, Putrus GA, Smith KS. Evaluation of the effects of rotor harmonics in a doubly-fed induction generator with harmonic induced speed ripple. *Trans Energy Conv.* 2003;18:508-515.
23. Hamby DM. A review of techniques for parameter sensitivity analysis of environmental models. *Environ Monit Assess.* 1994;32:135-154.
24. Saltelli A, Tarantola S, Campolongo F, Ratto M. *Sensitivity Analysis in Practice a guide to assessing scientific models.* Chichester, West Sussex, England: John Wiley & Sons Ltd; 2004.
25. Saraiva JP, Lima BS, Gomes VM, et al. Calculation of sensitivity index using one-at-a-time measures based on graphical analysis. Paper presented at: 18th International Scientific Conference on Electric Power Engineering (EPE); 2017.
26. Kundur P. *Power System Stability and Control.* New York: McGraw-Hill; 1993.
27. Krause PC, Wasynczuk O, Sudhoff SD. *Analysis of Electric Machinery and Drive Systems.* New York: John Wiley & Sons Ltd; 2002.
28. White KL, Chaubey I. Sensitivity analysis, calibration and validation for a multisite and multivariable SWAT model. *J Am Water Res Assoc.* 2005;41(5):1077-1089.
29. Santos L, Silva C, Paiva J, et al. A methodology for calculation of complexity in systems: case study. Paper presented at: IEEE Congreso Chileno de Ingeniería Eléctrica, Electrónica, Tecnologías de la Información y Comunicaciones; 2015.
30. Salas EAL, Henebry GM. A new approach for the analysis of hyperspectral data: theory and sensitivity analysis of the moment distance method. *Remote Sens.* 2014;6:20-41.
31. Frey HC, Patil SR. Identification and review of sensitivity analysis methods. *Risk Anal.* 2002;22:553-578.
32. Helton JC, Johnson JD, Sallaberry CJ, Storlie CB. Survey of sampling-based methods for uncertainty and sensitivity analysis. *Reliab Eng Syst Safe.* 2006;91:1075-1209.
33. Gomes VM, Saraiva JP, Lima BS, et al. Analytical method for calculating the sensitivity index of system parameters. Paper presented at: IEEE Congreso Chileno de Ingeniería Eléctrica, Electrónica, Tecnologías de la Información y Comunicaciones; 2017.
34. Magalhães AS, Bulhões JS, Matias CA, et al. Sensitivity analysis of the synchronous generation repowering system in parallel with induction generator. Paper presented at: IEEE Congreso Chileno de Ingeniería Eléctrica, Electrónica, Tecnologías de la Información y Comunicaciones; 2017.
35. Rashid MH. *Power Electronics: Circuits, Devices, and Applications.* Harlow, Essex, UK: Pearson Education Ltd, 2013.
36. Chapman SJ. *Electric Machinery Fundamentals.* New York: McGraw-Hill; 1991.
37. Fenger M, Campbell S, Pedersen J. Motor winding problems caused by inverter drives. *IEEE Ind Applicat Mag.* 2003;9:22-31.

How to cite this article: Magalhaes AS, Bulhoes JS, Reis MRC, et al. Experimental study of induction generator as a repowering solution. *Int Trans Electr Energy Syst.* 2020;30:e12365. <https://doi.org/10.1002/2050-7038.12365>